Journal of Molecular and Cellular Cardiology Plus 8 (2024) 100072

Contents lists available at ScienceDirect

Journal of Molecular and Cellular Cardiology Plus

journal homepage: www.journals.elsevier.com/journal-of-molecular-andcellular-cardiology-plus

The selective serotonin reuptake inhibitor paroxetine improves right ventricular systolic function in experimental pulmonary hypertension

Mark T. Waddingham [a,*], Hirotsugu Tsuchimochi [a], Takashi Sonobe [a,b], Vasco Sequeira [a,c], Md Junayed Nayeem [a], Mikiyasu Shirai [a], James T. Pearson [a,d,*,1], Takeshi Ogo [e,1]

[a] Department of Cardiac Physiology, National Cerebral and Cardiovascular Center, Suita, Osaka, Japan
[b] Department of Bioregulatory Science, Graduate School of Medicine, Nippon Medical School, Tokyo, Japan
[c] DZHI, Department of Translational Science Universitätsklinikum, Würzburg, Germany
[d] Department of Physiology, Victoria Heart Institute, Monash Biomedical Discovery Institute, Monash University, Clayton, VIC, Australia
[e] Division of Pulmonary Circulation, Department of Cardiovascular Medicine, National Cerebral and Cardiovascular Center, Suita, Osaka, Japan

ARTICLE INFO

Keywords:
Pulmonary hypertension
Right ventricular function
Paroxetine
Selective serotonin reuptake inhibitor
Myofilament protein phosphorylation
G protein-coupled receptor kinase 2 (GRK2)
Sympathetic nervous system

ABSTRACT

Background: Pulmonary hypertension (PH) often leads to right ventricle (RV) failure, a significant cause of morbidity and mortality. Despite advancements in PH management, progression to RV maladaptation and subsequent failure remain a clinical challenge. This study explored the effect of paroxetine, a selective serotonin reuptake inhibitor (SSRI), on RV function in a rat model of PH, hypothesizing that it improves RV function by inhibiting G protein-coupled receptor kinase 2 (GRK2) and altering myofilament protein phosphorylation.
Methods: The Su5416/hypoxia (SuHx) rat model was used to induce PH. Rats were treated with paroxetine and compared to vehicle-treated and control groups. Parameters measured included RV morphology, systolic and diastolic function, myofilament protein phosphorylation, GRK2 activity, and sympathetic nervous system (SNS) markers.
Results: Paroxetine treatment significantly improved RV systolic function, evidenced by increased stroke volume, cardiac output, and ejection fraction, without significantly affecting RV hypertrophy, myosin heavy chain/titin isoform switching, or fibrosis. Enhanced phosphorylation of titin and myosin light chain-2 was observed, correlating positively with improved systolic function. Contrary to the hypothesis, improvements occurred independently of GRK2 inhibition or SNS modulation, suggesting an alternate mechanism, potentially involving antioxidant properties of paroxetine.
Conclusion: Paroxetine improves RV systolic function in PH rats, likely through mechanisms beyond GRK2 inhibition, possibly related to its antioxidant effects. This highlights the potential of paroxetine in managing RV dysfunction in PH, warranting further investigation into its detailed mechanisms of action and clinical applicability.

1. Introduction

Recent advances in clinical medicine have enhanced the management of pulmonary hypertension (PH) by utilizing new generation vasodilator therapies, which have improved patient outcomes. Nevertheless, some patients still succumb to right ventricle (RV) failure as a result of the excessive afterload placed upon the RV that is associated with chronic PH. Initially, the RV will undergo adaptive remodeling whereby hypertrophy of the RV myocardium serves to maintain cardiac output and pulmonary flow [1,2]. In the long term however, a sustained increase in RV afterload drives maladaptive remodeling that is associated with dilatation, myocardial dysfunction, increased oxygen and energetic demand of the RV that all leads to RV failure and eventual patient death [1,2].

It is largely accepted that overactivation of the sympathetic nervous system is involved in preserving RV myocardial function and cardiac output in PH but ultimately induces pathological remodeling to the RV myocardium such as interstitial fibrosis, myosin heavy chain isoform

* Corresponding authors at: Department of Cardiac Physiology, National Cerebral and Cardiovascular Center, 6-1 Kishibe-shinmachi, Suita-shi, 564-8565, Osaka, Japan.
E-mail addresses: mtwaddingham@ncvc.go.jp (M.T. Waddingham), jpearson@ncvc.go.jp (J.T. Pearson).
[1] These authors contributed equally and share senior authorship.

https://doi.org/10.1016/j.jmccpl.2024.100072
Received 1 February 2024; Received in revised form 13 March 2024; Accepted 24 March 2024
Available online 26 March 2024

switching and impaired Ca^{2+} handling, driving the development of overt systolic and diastolic dysfunction and the evolution of RV failure [3]. Clinical [4] and several in vivo experimental studies in either the monocrotaline [5–7] or Su5416/hypoxia [8] rat models of PH have demonstrated a clear benefit of sympathetic nervous system (SNS) blockade in improving RV function, with variable effects upon pulmonary vascular remodeling and pulmonary artery pressure. More specifically, at the level of the myofilament, heightened SNS activity initially promotes the activation of the protein kinase A (PKA) pathway that enhances RV contractility through the phosphorylation of key sarcomeric proteins such as cardiac troponin I (cTnI), cardiac myosin binding protein-C (cMyBP-C), myosin light chain-2 (MLC-2) and titin along with Ca^{2+} handling proteins [9]. Nonetheless, prolonged SNS activation causes a reduction in β-adrenergic sensitivity that conversely diminishes PKA-mediated phosphorylation [9]. Alterations in myofilament post-translational modifications have been demonstrated in RV myocardial tissue acquired from patients with pulmonary arterial hypertension (PAH) undergoing heart transplantation, where substantial reductions in cTnI, cMyBP-C and titin phosphorylation have been reported compared to the donor samples [10]. The impact of SNS overactivation upon RV myofilaments is further highlighted in the setting of PH where chronic β-adrenoceptor blockade with bisoprolol was associated with improved RV systolic and diastolic function and enhanced cTnI and cMyBP-C phosphorylation [5].

Emerging novel evidence indicates that overactivation of G protein-coupled receptor kinase 2 (GRK2) is also widely implicated in the development of heart failure, principally through the internalization of β-adrenoceptors, desensitization of the myocardium to SNS signaling and promoting SNS overdrive [11,12]. However, GRK2 has also been found to impair cardiomyocyte fatty acid metabolism [13], disrupt mitochondrial metabolism [14] and negatively modulate nitric oxide signaling within cardiomyocytes [15]. These effects, combined with SNS desensitization/overdrive, may dramatically affect ventricular function via myofilament protein post-translational modifications. In rat models of RV hypertrophy and PH, GRK2 activation within the RV cardiomyocytes coincided with reductions in β_1-adrenoceptor density and myocardial cAMP concentration [16], suggesting that downstream PKA-mediated phosphorylation of myofilament proteins, namely cTnI, cMyBP-C and titin, may also be diminished and hence drive RV myocardial dysfunction in these models. Importantly, these data also indicate that GRK2 is an attractive target to enhance RV myocardial function in the setting of PH.

The selective serotonin reuptake inhibitor (SSRI), paroxetine, prescribed to manage depression in patients has been identified as a potent and highly selective inhibitor of GRK2 [17]. Chronic paroxetine treatment in both rat [18] and mouse [19] models of left heart dysfunction and failure have been reported to reduce cardiac hypertrophy, reduce myocardial interstitial fibrosis, restore β-adrenoceptor/SNS signaling and enhance myocardial function via a GRK2 inhibition. It is currently unknown whether the beneficial effects of chronic paroxetine treatment also extend to the myofilaments.

In this proof-of-concept study, we hypothesized that paroxetine treatment would improve RV myocardial function via the inhibition of GRK2, thereby preventing changes in the phosphorylation status of key myofilament proteins known to contribute to the development of RV dysfunction and failure in rats with PH induced by Su5416/hypoxia.

2. Methods

2.1. Animals and study design

Seven-week old, male Sprague-Dawley rats ($n = 32$) were sourced from Japan SLC (Shizuoka, Japan). Rats were subsequently randomized to the control ($n = 12$) or PH ($n = 20$) groups. In this study, PH was induced using the Su5416/chronic hypoxia (SuHx) method as previously described [20]. Rats in the SuHx group received a single subcutaneous injection of Su5416 (20 $mg \cdot kg^{-1}$; MedChemExpress, NJ, USA) suspended in a 0.5 % carboxymethylcellulose (CMC) solution (4 $mL \cdot kg^{-1}$) and placed in a hypoxia chamber (10 % O_2 by nitrogen mixing) for 3 weeks [20]. Subsequently, SuHx rats were maintained under normoxic conditions (room air) for a further 2 weeks before being further randomized to receive paroxetine hydrochloride ($n = 10$, 5 $mg \cdot kg^{-1} \cdot day^{-1}$; MedChemExpress) or vehicle (n = 10, 10 % DMSO, 40 % PEG-300, 5 % Tween-80, 45 % physiological saline) via a subcutaneously implanted osmotic minipump for 4 weeks (model 2ML4, Alzet®; Durect Corporation, CA, USA). Osmotic minipumps were surgically implanted in an aseptic manner under light isoflurane anesthesia (~1.5 % mixed in air with 100 % O_2) along the flank of the rat. Each rat was administered an analgesic for pain relief (carprofen, 5 $mg \cdot kg^{-1}$ s.c.; Zoetis, Tokyo, Japan) [20]. Control rats received an equivalent volume of the 0.5 % CMC solution (4 $mL \cdot kg^{-1}$) and were housed in normoxic conditions throughout the study (Supplementary Fig. 1). All rats were housed in a temperature and humidity-controlled environment and provided standard laboratory chow (CLEA Japan, Tokyo, Japan) and water ad libitum.

2.2. RV pressure-volume loop acquisition, hemodynamic measurements & analysis

At the conclusion of the study, all rats were subjected to hemodynamic evaluation and RV pressure-volume (PV) loop acquisition. Rats were anesthetized with isoflurane (3–4 % for induction; 1.5–2 % for maintenance) in oxygen-enriched air (~40 % O_2) and once deep surgical anesthesia was confirmed, underwent tracheal intubation and then mechanically ventilated with a respiratory rate 70–80 $breaths \cdot min^{-1}$ and a tidal volume of ~7 $mL \cdot kg^{-1}$. Body temperature was maintained at 37 °C ± 1 °C using a rectal thermocouple probe connected to a heating pad. The right jugular vein was cannulated for fluid replacement (Ringer's lactate, 5 $mL \cdot kg^{-1} \cdot h^{-1}$) and the right common carotid artery cannulated for the continuous measurement of systemic arterial blood pressure. RV catheterization was then performed using an open-chest approach. A full thoracotomy was performed to fully expose the heart and a 1.9Fr miniaturized PV catheter (Scisense, Ontario, Canada) was inserted into the RV along its long axis using an apical stab approach [21]. The ascending aorta was then carefully dissected away from the surrounding tissue and isolated so that a flow-probe (Model# 2.5PSB, Transonic, NY, USA) could be positioned to continuously measure cardiac output and calibrate the PV catheter volume signal. Loose ligatures were also placed around the inferior vena cava (IVC) to facilitate preload reduction. Rats were allowed to stabilize after the surgery (~5-10 min), prior to PV loop acquisition.

PV loops were recorded during steady-state and a subsequent occlusion of the IVC for the determination of load-insensitive indices of myocardial function. All recordings were made with ventilation briefly suspended at end inspiration (5–10s, tracheal pressure of ~10-12 cm H_2O) and after verifying the stability of the physiological parameters to avoid artefacts arising from catheter movement from breathing. Blood pressure data was acquired using a fluid-filled transducer (MLT0670; ADInstruments, NSW, Australia) and PV loop data using the ADV500 system (Scisense), both connected to a PowerLab 16/30 (ADInstruments) and recorded in LabChart Pro software (v.8.1.25, ADInstruments) at a sampling rate of 1000 Hz. PV loop and hemodynamic data analysis was performed off-line using the PV Loop Module and Blood Pressure Module within LabChart Pro (v.8.1.25, ADInstruments). Arterial elastance (Ea) was calculated as the RV end systolic pressure divided by stroke volume and RV stroke work was defined as the area of the PV loop. Total pulmonary resistance was calculated as the quotient of estimated mean pulmonary artery pressure ($0.61 \times RVSP + 2$) divided by cardiac output [22]. The RV relaxation time constant (Tau) was calculated using the Logistic method [23].

2.3. Tissue collection

Rats were killed after PV loop acquisition with an overdose of potassium chloride (i.v.) while under deep surgical anesthesia (5 % isoflurane). The heart was rapidly excised, rinsed in ice-cold 1 × PBS to remove excess blood, blotted dry and weighed. The RV was then separated from the LV and interventricular septum (LV + IVS), both were weighed and sliced along the transverse axis. The apical portion was minced, snap-frozen in liquid nitrogen and stored at −80 °C. The remainder was halved along the transverse axis, with one half fixed in 4 % paraformaldehyde and embedded in paraffin and the other half directly embedded in optimum cutting temperature (OCT) compound (Sakura Finetek®, Tokyo, Japan), frozen in cooled isopentane and stored at −80 °C. Tibia length was measured as an index of body size.

2.4. Histology

RV tissue sections of 4 μm were dewaxed in two changes of xylene and rehydrated to water through graded ethanols (2 × 100 %, 1 × 90 %, 1 × 80 %, 1 × 70 %) for 3 min each. Paraffin-embedded sections were stained with hematoxylin and eosin (H&E) to assess cardiomyocyte cross-sectional area. Cryosections were stained with picrosirius red to demonstrate RV interstitial collagen per the manufacturers' instructions (Polysciences Inc., PA, USA). All slides were imaged using a digital slide scanner (NanoZoomer S60, Hamamatsu Photonics, Hamamatsu, Japan) and analyzed using Aperio ImageScope (v12.3; Leica Biosystems, Wetzlar, Germany) [24].

2.5. Tissue preparation for SDS-PAGE

2.5.1. Whole RV lysates

Approximately 50 mg of RV tissue was homogenized in 350 μL of ice-cold RIPA lysis buffer (Abcam, Cambridge, UK) containing protease (cOmplete™ mini cocktail, Roche, Basel, Switzerland) and phosphatase (PhosSTOP™, Roche) inhibitors with a mechanical homogenizer and incubated on ice for 30 min. Homogenates were centrifuged at 20,000*g* at 4 °C for 30 min and the supernatant collected as the whole RV lysate. Lysates were then immediately mixed 1:1 in 2 × Laemmli sample buffer (LSB; Bio-Rad, CA, USA) containing dithiothreitol (DTT; Roche) at a final concentration of 75 mM, heated at 95 °C for 5 min, cooled on ice and stored at −80 °C.

2.5.2. Myocardial tissue sub-cellular fractionation

RV tissue was homogenized in ice-cold standard relaxing buffer (SRB; 60 mM KCl, 30 mM Imidazole, 2 mM $MgCl_2$, 2 mM EDTA, 1 mM NaN_3 pH 7.4) [25] containing protease and phosphatase inhibitors (as above) using a mechanical homogenizer at a ratio of 10 μL to 1 mg of tissue [25]. Homogenates were centrifuged at 20,000*g* for 2 min at 4 °C, with the supernatant designated as the cytosolic fraction. The pellet was resuspended in ice-cold SRB with the addition of 1 % Triton X-100 (SRBX-100), incubated on ice for 15 min with frequent vortexing and centrifuged at 20,000*g* for 2 min at 4 °C. The supernatant was designated as the membrane fraction. After washing the pellet twice in 1 mL of SRBX-100 and once more in 1 mL of SRB to remove the Triton X-100 by vortexing and centrifugation as above, the final pellet was resuspended in sample buffer (8 M Urea, 2 M Thiourea, 10 % Glycerol, 3 % SDS, 0.05 M Tris-HCl pH 6.8, 75 mM DTT, 0.005 % bromophenol blue) at a ratio 5 μL to 1 mg of the original tissue weight, heated at 60 °C for 10 min and centrifuged at 20,000 *g* for 15 min at 4 °C, with the supernatant being designated as the myofilament fraction [25]. Protein from the cytosolic and membrane fractions were subsequently precipitated by the addition of four volumes ice-cold methanol, one volume of ice-cold chloroform and four volumes of ice-cold dH_20, vortexed thoroughly and centrifuged at 20,000 *g* for 5 min at 4 °C. The upper phase was discarded, and the white protein pellet and lower phase were resuspended in ice-cold methanol and centrifuged as before. The supernatant was then decanted, and the pellet air-dried for 30 min. Protein pellets were then resuspended in sample buffer, heated and centrifuged as per the myofilament fraction. All samples were stored at −80 °C.

2.5.3. Protein concentration estimation

The protein concentration of each sample was estimated using the Pierce™ 660 nm Protein Assay (Thermo Fisher Scientific, MA, USA) as previously described [24]. Diluted samples (5- to 10-fold) were compared against a standard curve of known concentrations. For samples solubilized in sample buffer, the protein assay reagent was supplemented with ionic detergent compatibility reagent (IDCR, Thermo Fisher Scientific). The absorbance values were read at 660 nm using a POLARstar OMEGA microplate reader (BMG Labtech, Offenburg, Germany).

2.6. Myofilament protein phosphorylation

5 μg of RV myofilament protein (see above) was loaded onto gradient 5–20 % acrylamide pre-cast mini gels (SuperAce™ Ace, FUJIFILM Wako Pure Chemicals, Tokyo, Japan) and subjected to SDS-PAGE under reducing conditions at a constant 20 mA until the dye-front reached the bottom of the gel. The gels were then fixed, washed, stained with Pro-Q Diamond Phosphoprotein Stain (Invitrogen), destained and washed as previously described [24]. Gels were imaged using an Amersham Imager 680 with a Cy3 fluorescence protocol (Cytiva, MA, USA). Gels were then post-stained for total protein with Coomassie blue solution (InstantBlue®, Abcam, Cambridge, UK) for 1 h, destained in several changes of dH_2O and imaged with an Amersham Imager 680 (Cytiva). Band densities were analyzed using Image Lab (v6.0.1, Bio-Rad, CA, USA).

2.7. Titin isoform determination & phosphorylation

Titin isoform and relative phosphorylation were determined by utilizing vertical SDS agarose gel electrophoresis [26]. 10 μg of RV myofilament protein per sample (see above) was loaded onto 16 cm × 16 cm × 2 cm 1 % agarose gels and ran under reducing conditions at a constant 16 mA for 4 h, with cooling. Rat tibialis anterior (TA) muscle was also loaded as a reference for the N2A titin isoform. For isoform determination, gels were fixed and then stained in SYPRO Ruby (Invitrogen, OR, USA) overnight with gentle agitation and imaged using an Amersham Imager 680 (Cytiva, MA, USA). For relative phosphorylation, agarose gels were stained with Pro-Q Diamond and imaged with a Cy3 fluorescence protocol (see above). Gels were then post-stained overnight in SYPRO Ruby to assess total protein an imaged as above. Band densities were analyzed using Image Lab (v6.0.1, Bio-Rad, CA, USA).

2.8. Myosin heavy chain isoform determination

2 μg of RV myofilament protein per sample was loaded onto a 16 cm × 16 cm × 1 cm 6 % polyacrylamide gel and run at a constant 16 mA for 5 h [27]. The gel was subsequently stained in Coomassie blue solution (InstantBlue®, Abcam, Cambridge, UK) for 1 h, destained in several changes of dH_2O and imaged by transillumination with an Amersham Imager 680 (Cytiva, MA, USA). Band densities were analyzed using Image Lab (v6.0.1, Bio-Rad, CA, USA).

2.9. Western blotting

5-10 μg of protein per sample were loaded onto either gradient (5–20 %) or 10 % acrylamide pre-cast mini gels (SuperAce™ Ace, FUJIFILM Wako Pure Chemicals, Tokyo, Japan) and subjected to SDS-PAGE under reducing conditions at a constant 20 mA/gel until the dye-front reached the bottom of the gel. Proteins were then transferred to PVDF membranes with a semi-dry technique (TransBlot Turbo™, Bio-Rad, CA, USA) and stained with Ponceau-S (Sigma-Aldrich, MO, USA) to

confirm protein transfer and serve as the loading control. Membranes were then washed in 1 × TBST and blocked for 1 h at room temperature in blocking solution (Blocking One, Nacalai Tesque, Kyoto, Japan). After washing in 1 × TBST, membranes were incubated in primary antibody at 4 °C overnight against the following proteins: GRK2 (1:2000; Novus Biologicals, NBP2–37611), β_1AR (1:100, Santa Cruz Biotechnology, sc-568), tyrosine hydroxylase (1:1000; GeneTex, GTX113016), phospho-cMyBP-C^{Ser282} (1:1000; Enzo Lifesciences, ALX-215-057-R050), phospho-cTnI$^{Ser23/24}$ (1:1000, Cell Signaling Technologies, 4004), phospho-MLC-2v^{Ser15} (1:1000; GenTex, GTX17513), total cMyBP-C (1:1000, Santa Cruz Biotechnology, sc-137,180), total cTnI (1:1000; Cell Signaling Technologies, 4002) and total MLC-2v (1:1000, Cell Signaling Technologies, 12,975). All primary antibodies were prepared in diluted blocking solution. The next day, membranes were washed for 4 × 10 min in 1 × TBST before being incubated either a goat anti-rabbit (β_1AR, tyrosine hydroxylase, phospho-cMyBP-C^{Ser282}, phospho-cTnI$^{Ser23/24}$, phospho-MLC-2v^{Ser15}, total cTnI and total MLC-2v) or goat anti-mouse (GRK2 and total cMyBP-C) secondary antibody (both diluted 1:2500 in diluted blocking solution; Agilent, CA, USA) for 1 h at room temperature. Membranes were then washed again 3x5min in 1xTBST, incubated in ECL solution (ECL Prime; Cytiva, MA, USA) and then imaged using an Amersham Imager 680 (Cytiva). Band densities were analyzed using Image Lab (v6.0.1, Bio-Rad, CA, USA).

2.10. High performance liquid chromatography (HPLC)

RV myocardial catecholamine stores were measured by HPLC-ECD (HTEC-500, Eicom) as previously described [28]. Briefly, a small piece of snap-frozen RV myocardium was homogenized in 0.1 M perchloric acid using a hand-held homogenizer (Power Masher II, Nippi Protein Engineering, Tokyo, Japan), centrifuged at 20,000 *g* for 15 min at 0 °C and the supernatant saved. After adjusting the pH to ~3.0 with the addition of 1 M sodium acetate solution, the supernatant underwent ultrafiltration using a 10,000-MW cut-off membrane filter (Ultrafree MC; Merck Millipore, Tokyo, Japan). The ultrafiltrate was then directly injected into HPLC system for the measurement of the catecholamines dopamine, norepinephrine and epinephrine.

2.11. Statistical analysis

All data are presented as mean with error bars representing the standard error of the mean (SEM) and *n* indicating the number of animals in each group. A one-way ANOVA was carried out to establish differences between the groups. A Bonferroni's post hoc test was used to correct for multiple comparisons. Correlations between independent and dependent variables were established using linear regression. Statistical analysis was performed using GraphPad Prism (v9.5, GraphPad, CA, USA). A *p*-value of <0.05 was considered statistically significant.

3. Results

3.1. General animal characteristics & RV morphology

When compared to the control group, vehicle-treated SuHx rats exhibited significantly lower body weight ($p < 0.0001$), along with a significantly higher normalized heart ($p < 0.0001$), LV + IVS ($p < 0.001$) and RV ($p < 0.0001$) weights (Table 1). RV weight relative to LV + IVS weight (Fulton Index) was also significantly greater in vehicle-treated SuHx rats in comparison to the control group ($p < 0.0001$, Table 1). Chronic treatment of SuHx rats with paroxetine, resulted in higher body weight compared to the vehicle-treated SuHx rats ($p < 0.05$, Table 1) although paroxetine had no effect upon relative heart, LV + IVS or RV weights as well as the Fulton Index (Table 1). In regards to RV morphology, vehicle-treated SuHx rats demonstrated remarkably greater RV cardiomyocyte cross-sectional area when compared to control rats ($p < 0.0001$ vs. Control, Fig. 1A) in addition to a modest but significantly elevated RV interstitial fibrotic area fraction ($p < 0.05$ vs. Control, Fig. 1B). Paroxetine treatment of SuHx rats did not significantly alter RV cardiomyocyte cross-sectional area (Fig. 1A) or the RV interstitial fibrotic area fraction when compared to vehicle-treated SuHx rats (Fig. 1B).

Table 1
General animal characteristics and morphometrics of control, SuHx+vehicle and SuHx+paroxetine rats at the conclusion of the study.

	Control	SuHx+vehicle	SuHx+paroxetine
n	12	8	6
General animal characteristics			
Body weight (g)	473 ± 10	361 ± 20$^{\#\#}$	429 ± 23†
Tibia length (mm)	43 ± 0.3	40 ± 0.5**	40 ± 0.8**
Morphometrics			
Heart weight:tibia length (mg·mm^{-1})	25 ± 0.5	46 ± 1.5$^{\#\#}$	45 ± 2.2$^{\#\#}$
RV weight:tibia length (mg·mm^{-1})	4.5 ± 0.1	13.9 ± 0.5$^{\#\#}$	14.1 ± 0.9$^{\#\#}$
LV + IVS weight:tibia length (mg·mm^{-1})	18.1 ± 0.4	23.2 ± 0.9$^{\#}$	23.0 ± 1.0$^{\#}$
Fulton Index (RV/LV + IVS)	0.24 ± 0.01	0.61 ± 0.03$^{\#\#}$	0.61 ± 0.04$^{\#\#}$

Data are express as mean ± SEM. A one-way ANOVA was used to establish differences among the groups with a Bonferroni's post hoc test to correct for multiple comparisons. RV: Right ventricle, LV + IVS: left ventricle + interventricular septum.
** $p < 0.01$.
$^{\#}$ $p < 0.001$.
$^{\#\#}$ $p < 0.0001$ vs. Control.
† $p < 0.05$ vs. SuHx+Vehcile.

3.2. RV systolic dysfunction associated with PH is improved by paroxetine treatment

Upon anesthesia and catheterization, vehicle-treated SuHx rats exhibited a significantly reduced heart rate ($p < 0.05$ vs. Control) as well as elevated RV end systolic pressure ($p < 0.001$ vs. Control), RV afterload (Arterial elastance; $p < 0.0001$ vs. Control) and total pulmonary resistance ($p < 0.0001$ vs. Control), indicating the development of severe PH (all Table 2). Vehicle-treated SuHx rats exhibited pronounced RV systolic dysfunction, evident by a significantly lower stroke volume ($p < 0.05$), cardiac output ($p < 0.01$) and a near-significant ~30 % reduction in ejection fraction ($p = 0.07$) compared to the Control group (all Table 2). RV diastolic dysfunction was also observed in the vehicle-treated SuHx rats with a significant increase end diastolic pressure ($p < 0.05$ vs. Control, Table 2) and a prolongation of the relaxation time constant, Tau (Tau Logistic; $p < 0.01$ vs, Control, Table 2).

Paroxetine treatment of SuHx rats was associated with significantly lower RV afterload (Arterial elastance; $p < 0.05$ vs. SuHx+Vehicle, Table 2) and total pulmonary resistance ($p < 0.05$ vs. SuHx+Vehicle, Table 2) by comparison to the SuHx+Vehicle group (Table 2). RV systolic function was also enhanced in SuHx rats treated with paroxetine as demonstrated by a significantly greater stroke volume ($p < 0.05$ vs. SuHx+Vehicle, Table 2), a near significant increase of cardiac output ($p = 0.07$ vs. SuHx+Vehicle, Table 2) and a ~ 20 % higher ejection fraction although this difference did not reach statistical significance (Table 2). Importantly, paroxetine treatment of SuHx also significantly enhanced the RV stroke work compared to the vehicle-treated SuHx rats ($p < 0.05$ vs. SuHx+Vehicle, Table 2) suggesting that paroxetine treatment may indeed directly improve the pump function against sustained afterload in the RV of PH rats (Table 2). Despite these improvements in RV systolic function, diastolic function was not affected by paroxetine treatment in SuHx rats (Table 2).

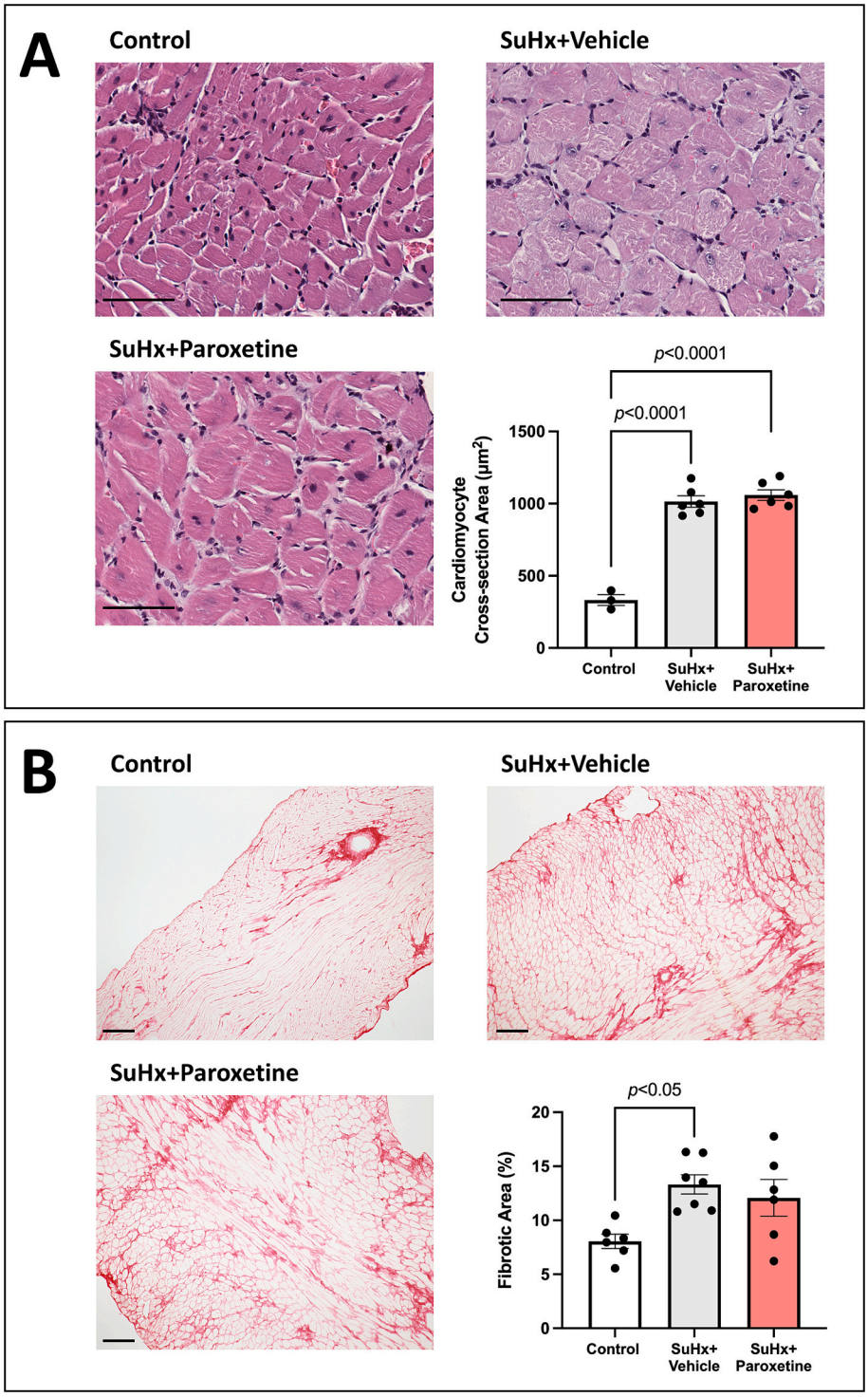

Fig. 1. Chronic paroxetine treatment did not affect the RV cardiomyocyte hypertrophy or the development of RV myocardial interstitial fibrosis associated with PH in the SuHx rats. **A:** Representative photomicrographs (x40 objective) of hematoxylin and eosin stained RV sections from Control ($n = 3$), SuHx+Vehicle ($n = 6$) and SuHx+Paroxetine (5 mg·kg^{-1}·day^{-1}, n = 6) rats. When compared to control, both vehicle- and paroxetine-treated SuHx exhibited a significantly increased cardiomyocyte cross-sectional area (both $p < 0.001$ vs. Control). The lower right panel shows the average cross-sectional area of at least 20 RV myocytes measured from each section (animal) per group. **B:** Representative photomicrographs (x10 objective) RV cryosections stained with picrosirius red to demonstrate the extracellular matrix and interstitial collagen (fibrosis) in Control (n = 6), SuHx+Vehicle ($n = 7$) and SuHx+Paroxetine (n = 6). PH in SuHx+Vehicle rats was associated with a significant increase in the fibrotic area (red staining) compared to Controls ($p < 0.05$). Paroxetine-treatment of SuHx rats resulted in a slightly lower fibrotic area compared to vehicle-treated SuHx rats (NS). Data are presented as mean ± SEM. A one-way ANOVA with a Bonferroni's post hoc test was used to assess differences between the groups. Scale bars in A and B indicate 50 μm. (For interpretation of the references to colour in this figure legend, the reader is referred to the web version of this article.)

Table 2
RV steady-state functional indices from control, SuHx+vehicle and SuHx+paroxetine rats at the conclusion of the study.

n	Control	SuHx+ Vehicle	SuHx+ Paroxetine	One-Way ANOVA with a Bonferroni's Post Hoc Test (*p*-value)		
	6	7	6			
Hemodynamics				Control vs. SuHx+Vehicle	Control vs. SuHx+Paroxetine	SuHx+Vehicle vs. SuHx+Paroxetine
Mean arterial pressure (mmHg)	87 ± 6	88 ± 6	76 ± 7	NS	NS	NS
Heart rate (BPM)	305 ± 16	255 ± 6	271 ± 14	$p < 0.05$	NS	NS
Arterial elastance (mmHg·μL^{-1})	0.12 ± 0.01	0.84 ± 0.05	0.64 ± 0.07	$p < 0.0001$	$p < 0.001$	$p < 0.05$
Total pulmonary resistance (mmHg·μL^{-1}·min^{-1})	0.28 ± 0.02	2.10 ± 0.17	1.38 ± 0.25	$p < 0.0001$	$p < 0.01$	$p < 0.05$
Right ventricular systolic function						
End systolic pressure (mmHg)	24 ± 1	96 ± 3	95 ± 4	$p < 0.0001$	$p < 0.0001$	NS
End systolic volume (μL)	169 ± 22	237 ± 50	217 ± 25	NS	NS	NS
Stroke volume (μL)	204 ± 9	116 ± 6	162 ± 19	$p < 0.05$	NS	$p < 0.05$
Stroke work (mmHg·μL)	4796 ± 387	10,529 ± 730	15,918 ± 1982	$p < 0.05$	$p < 0.0001$	$p < 0.05$
Cardiac output (mL·min^{-1})	63 ± 6	30 ± 2	44 ± 6	$p < 0.01$	NS	$p = 0.07$
Ejection fraction (%)	57 ± 4	40 ± 5	48 ± 5	$p = 0.07$	NS	NS
dP/dt_{max} (mmHg·s^{-1})	1849 ± 101	4012 ± 188	4127 ± 186	$p < 0.0001$	$p < 0.0001$	NS
Right ventricular diastolic function						
End diastolic pressure (mmHg)	4.2 ± 0.6	7.1 ± 0.6	6.2 ± 0.7	$p < 0.05$	NS	NS
End diastolic volume (μL)	358 ± 23	318 ± 47	391 ± 37	NS	NS	NS
dP/dt_{min} (mmHg·s^{-1})	−1101 ± 59	−3809 ± 200	−3840 ± 203	$p < 0.0001$	$p < 0.0001$	NS
Tau logistic (ms)	7.3 ± 0.4	9.9 ± 0.4	8.8 ± 0.7	$p < 0.01$	NS	NS

Data are express as mean ± SEM. A one-way ANOVA was used to establish differences among the groups with a Bonferroni's post hoc test to correct for multiple comparisons.

3.3. Paroxetine enhances RV-PA coupling in SuHx rats

A sequential series of RV PV loops were acquired during IVC occlusions to obtain load-insensitive indices of RV systolic and diastolic function (Fig. 2A-C). The fitted end diastolic pressure-volume relationship (EDPVR, blue line Fig. 2A-C) was expressed using the exponential model: $P = \alpha \times (e^{\beta V - 1})$ with β being the RV stiffness constant and α the stiffness and scaling coefficient [29,30]. Compared to control rats, vehicle-treated SuHx rats exhibited a greater RV stiffness constant (β) of the EDPVR (EDPVR β, $p = 0.07$ vs. Control, Fig. 2A-D). Although there was an ~35 % lower EDPVR β in the SuHx+Paroxetine group compared to the SuHx+Vehicle group, this difference was not statistically significant (Fig. 2D). As the stiffness constant β does not account for the contribution of the stiffness and scaling coefficient α to global RV diastolic stiffness (i.e. EDPVR), end diastolic elastance (Eed) was calculated the as the slope of the EDPVR at end diastole with the formula: $\alpha \times \beta \times e^{(\beta \times EDV)}$ [30]. Eed was significantly elevated in the RV of vehicle-treated SuHx rats compared to the control rats ($p < 0.05$, Fig. 2D). In the paroxetine-treated SuHx rats, Eed was increased to a similar extent as the vehicle-treated SuHx rats compared to the control group, however the difference did not reach statistical significance (Fig. 2D). Overall, paroxetine treatment had little effect on the increased RV diastolic stiffness associated with PH in the SuHx rats (Fig. 2A-D).

The end systolic pressure-volume relationship (ESPVR, red line Fig. 2A-C), a load-insensitive index of ventricular contractile performance [31] was significantly higher in both the vehicle- and paroxetine-treated SuHx rats by comparison to control rats, demonstrating enhanced contractility against greater RV afterload in SuHx-treated rats (both $p < 0.05$ vs. Control, Fig. 2A-D). To further evaluate the intrinsic pump function of the RV relative afterload (so-called RV-pulmonary artery (PA) coupling), the slope of the ESPVR was expressed as a ratio with arterial elastance [32] (Table 2). When compared to control rats, vehicle-treated SuHx rats had an ~40 % reduction in the RV-PA coupling factor, consistent with impaired RV pump function (Fig. 2D). Paroxetine-treated SuHx rats on the other hand exhibited a marked ~45 % mean increase in the RV-PA coupling factor, in effect normalizing RV-PA coupling to values similar to control rats (Fig. 2D). It is important to note however that due to large variation in the data, no statistically significant differences were found among the groups for RV-PA coupling.

3.4. Altered titin and myosin isoform expression patterns in SuHx rats are unchanged by chronic paroxetine treatment

Titin isoform analysis of RV myofilament fractions revealed that control rats expressed an N2BA:N2B isoform ratio of around 40:60, where the stiffer N2B isoform is predominant (Fig. 3A&C). In the RV of vehicle-treated SuHx rats, a significant increase in the N2BA:N2B isoform ratio was observed at around 70:30 ($p < 0.001$ vs. Control, Fig. 3A&C), representing a primary titin isoform shift towards the more compliant N2BA. Paroxetine treatment of SuHx rats had no significant effect on the RV titin isoform expression ratio (75:25, Fig. 3A&C). Similarly, the myosin heavy chain (MHC) composition ratio was significantly altered in the RV of SuHx rats (Fig. 3B&D). Compared to control rats, vehicle-treated SuHx rats exhibited a significant increase of fetal-neonatal β-MHC isoform expression (31 % vs. 62 %, $p < 0.0001$, Fig. 3B&D), consistent with the development of heart failure in rodents. In SuHx rats treated with paroxetine, there was no significant difference in the β-MHC isoform expression compared to the vehicle-treated SuHx rats (65 % vs. 63 %, Fig. 3B&D).

3.5. Chronic paroxetine treatment of SuHx rats prevented changes in RV myofilament protein phosphorylation in SuHx rats

Analysis of the net (i.e. non-site specific) phosphorylation status of small myofilament proteins showed no significant differences of cMyBP-C, desmin, cTnT, cTm or cTnI relative phosphorylation among the groups (Fig. 4A&B). When compared to the control group, both the vehicle-treated and paroxetine-treated SuHx rats exhibited a significant reduction in net phosphorylation status of MLC-2 ($p < 0.01$ and $p < 0.05$ vs. Control, respectively; Fig. 4A&B). The net phosphorylation status of titin was also significantly reduced in the RV of vehicle-treated SuHx rats by comparison to control rats ($p < 0.001$, Fig. 4C&D), with chronic paroxetine treatment significantly enhancing net titin phosphorylation in the RV of SuHx rats ($p < 0.01$ vs. SuHx+Vehicle, Fig. 4C&D).

Site-specific analysis of RV small myofilament phosphoproteins

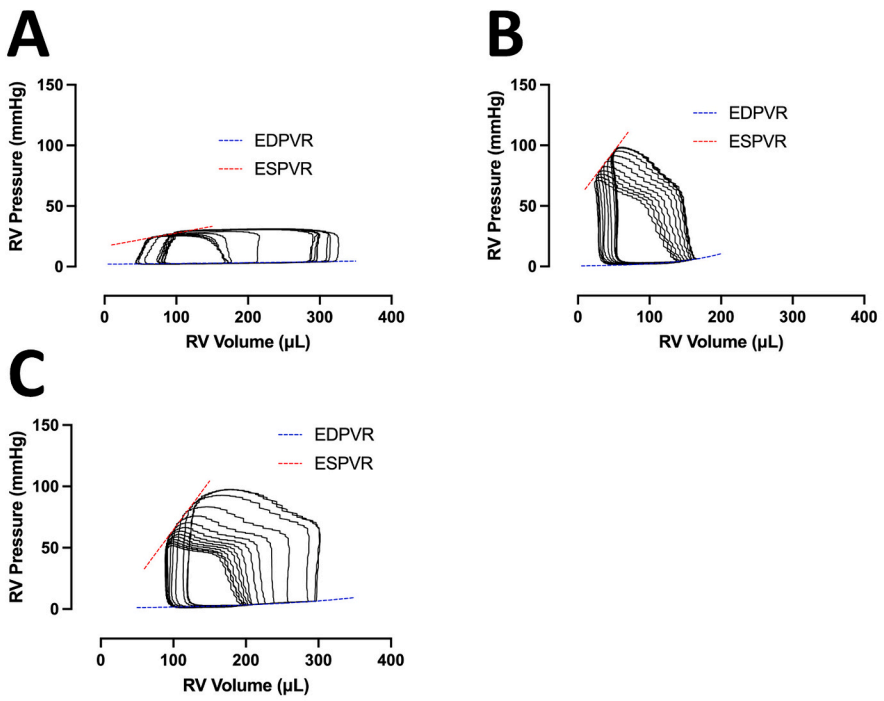

D

	Control	SuHx+ Vehicle	SuHx+ Paroxetine
n	6	7	6
EDPVR β (μL^{-1})	0.003±0.002	0.014±0.004	0.009±0.002
Eed (mmHg·μL^{-1})	0.01±0.002	**0.09±0.02***	0.08±0.02
Ees (mmHg·μL^{-1})	0.1±0.01	**0.53±0.08***	**0.51±0.12***
RV-PA Coupling (Ees·Ea^{-1})	0.85±0.05	0.62±0.08	0.96±0.22

Fig. 2. Chronic paroxetine treatment enhanced RV-PA coupling with no effect upon RV diastolic dysfunction in SuHx rats. Representative RV pressure-volume (PV) loop series acquired during inferior vena cava (IVC) occlusions in Control (**A**, n = 6), SuHx+Vehicle (**B**, n = 7) and SuHx+Paroxetine (**C**, n = 6). The EDPVR and ESPVR of each RV PV loop series (A-C) is indicated by the broken blue and red lines, respectively. **D** is a summary of the RV function indices calculated from the relationship of RV PV loops obtained during the IVC occlusions. When compared to the Control rats, both the SuHx groups exhibited higher RV diastolic stiffness, although this only reached statistical significance in the SuHx+Vehicle group ($p < 0.05$ vs. Control). Paroxetine treatment (5 $mg \cdot kg^{-1} \cdot day^{-1}$) of SuHx rats did not affect the slope of the ESPVR compared to vehicle-treated SuHx rats (both $p < 0.05$ vs. Control). The RV-PA coupling factor was reduced by ~40 % in the SuHx+Vehicle rats compared to Control, which was effectively normalized in the SuHx+Paroxetine group. Data are expressed as mean ± SEM. A one-way ANOVA with a Bonferroni's post hoc test was used to assess differences between the groups. *$p < 0.05$ vs. Control. EDPVR: end diastolic pressure-volume relationship; Eed: End diastolic elastance; Ees: End systolic elastance; RV-PA coupling: right ventricle-pulmonary artery coupling; Ea: Arterial elastance. (For interpretation of the references to colour in this figure legend, the reader is referred to the web version of this article.)

revealed a non-significant ~20 % lower relative phosphorylation of cMyBP-C at the serine 282 residue in both groups of SuHx rats when compared to controls (Fig. 5A). Additionally, there were no significant differences between the groups in terms of cTnI relative phosphorylation at the serine 23/24 site (Fig. 5B), indicating that the PKA-dependent myofilament phosphorylation was little different between the groups. Consistent with the net phosphorylation analysis, the relative phosphorylation of MLC-2 ventricular isoform (MLC-2v) was approximately 60 % lower at the serine 15 residue in the RV of vehicle-treated SuHx rats compared to controls ($p < 0.01$, Fig. 5C). Although the relative phosphorylation of MLC-2v was significantly lower than that of controls in the SuHx rats treated with paroxetine ($p < 0.05$, Fig. 5C), when compared the vehicle-treated SuHx rats, there was an almost 70 % enhanced relative phosphorylation of MLC-2v at the serine 15 site (MLC-2^{Ser15}) in the paroxetine-treated SuHx rats (Fig. 5C).

Importantly, pooled linear regression analysis revealed that changes in both RV MLC-$2v^{Ser15}$ and titin relative phosphorylation were associated with changes in RV systolic function. For instance, positive correlations were established between MLC-$2v^{Ser15}$ relative phosphorylation and stroke volume ($p = 0.06$, $r^2 = 0.241$, Fig. 5D), cardiac output ($p < 0.05$, $r^2 = 0.305$, Fig. 5E) and ejection fraction ($p < 0.05$, $r^2 = 0.376$, Fig. 5F). Positive correlations were also established between titin relative phosphorylation (Fig. 4C&D) and stroke volume ($p < 0.05$, $r^2 = 0.401$, Fig. 5G), cardiac output ($p < 0.01$, $r^2 = 0.45$, Fig. 5H) and ejection

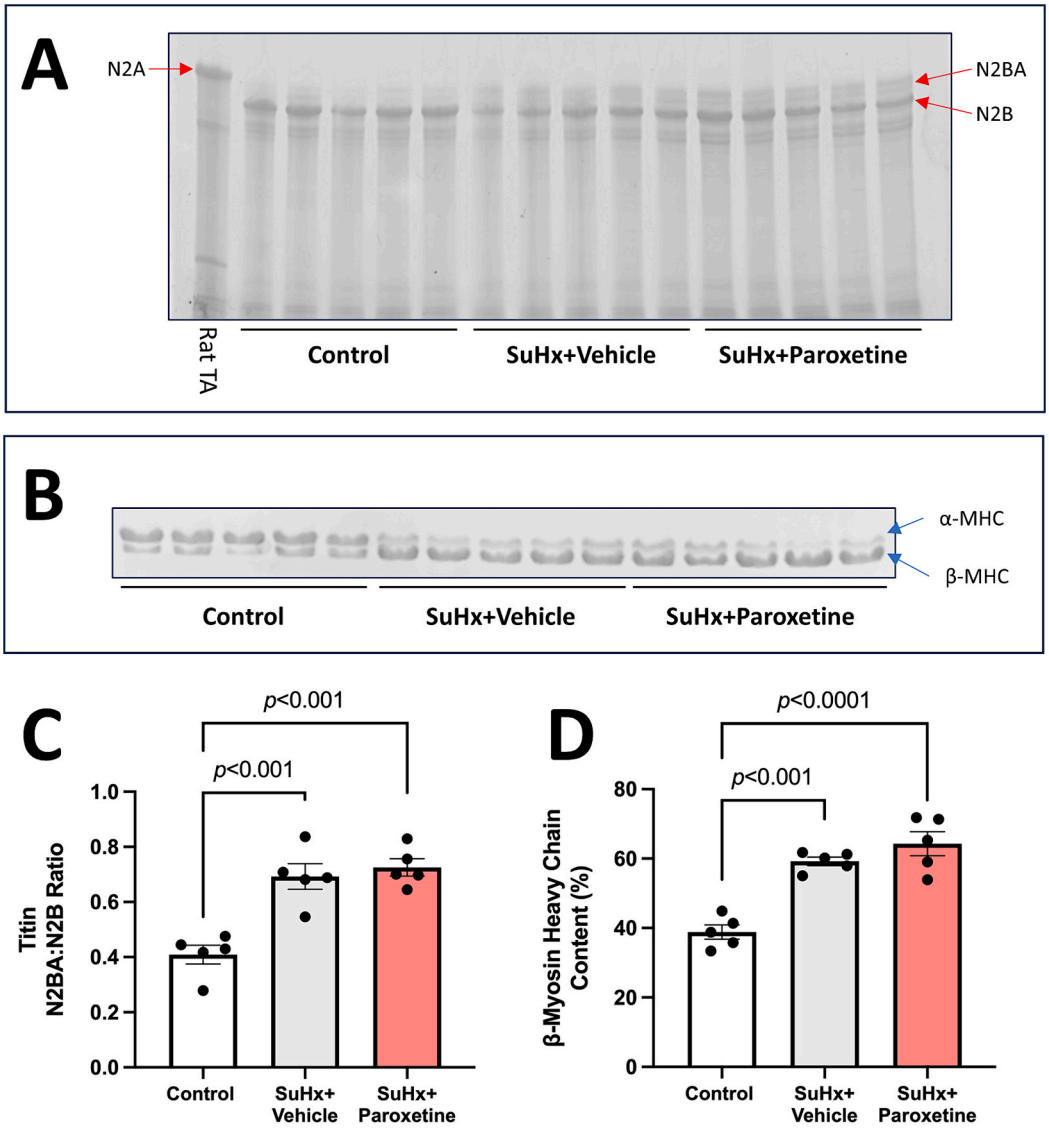

Fig. 3. Chronic paroxetine treatment did not influence altered titin or myosin heavy chain isoform composition in the RV. **A:** Representative image of a 1 % agarose gel stained with SYPRO Ruby and visualized using UV transillumination for Control ($n = 5$), SuHx+Vehicle (n = 5) and SuHx+Paroxetine (n = 5) rats. Rat tibialis anterior (TA) muscle was loaded as a reference of the longer skeletal muscle titin N2A isoform. **B:** Representative image of a 6 % polyacrylamide gel stained with Coomassie blue depicting separation of the α and β isoforms of myosin heavy chain (MHC) in Control ($n = 5$), SuHx+Vehicle (n = 5) and SuHx+Paroxetine (n = 5) rats. **C:** Quantification of the N2BA to N2B titin isoform ratio. Compared to controls, there was a significant increase in the titin N2BA:N2B isoform expression ratio in the vehicle-treated SuHx rats. Paroxetine treatment of SuHx rats (5 $mg \cdot kg^{-1} \cdot day^{-1}$) had no effect on the titin N2BA:N2B isoform expression ratio. **D:** Quantification of the relative expression of β-MHC in Control (n = 5), SuHx+Vehicle (n = 5) and SuHx+Paroxetine (n = 5) rats. PH in SuHx rats was associated with a significant increase in β-MHC content in the RV when compared to the Control rats ($p < 0.001$) that was not affected by paroxetine treatment ($p < 0.0001$ vs. Control). All samples were run simultaneously on one gel. Arrows indicate the bands that were analyzed for the corresponding protein label. Data are expressed as mean ± SEM. A one-way ANOVA with a Bonferroni's post hoc test was used to assess differences between the groups. TA: tibialis anterior, MHC: myosin heavy chain. (For interpretation of the references to colour in this figure legend, the reader is referred to the web version of this article.)

fraction ($p < 0.05$, $r^2 = 0.337$, Fig. 5I). These data demonstrate that the enhancements in myofilament phosphorylation observed in the paroxetine-treated SuHx rats are associated with improved RV systolic function.

3.6. Improvements in RV systolic function with paroxetine treatment in SuHx rats appear to be independent of GRK2 signaling and sympathetic nervous system modulation

In total RV protein homogenates, GRK2 expression was found to be ~30 % greater in the SuHx+Vehicle group when compared to the control group, although this difference did not reach statistical significance (Fig. 6A). GRK2 expression in total RV protein homogenates was also somewhat higher (~20 %) in the paroxetine-treated SuHx rats when compared to controls, however this difference was not statistically significant (Fig. 6A). Given that GRK2 translocates from the cytosol to the cell membrane upon activation, the relative proportion of the total GRK2 pool associated with the plasma membrane (translocation) was assessed in the RV (Fig. 6B). There was a significantly greater GRK2 translocation from the cytosol to the membrane in the vehicle-treated SuHx rats when compared to the control group ($p < 0.05$, Fig. 6B). Surprisingly, GRK2 translocation from the cytosol to the membrane was not affected by paroxetine treatment in SuHx rats ($p < 0.01$ vs. Control, Fig. 6B).

In both groups of SuHx rats, there was a minor decrease (~20 % lower, NS) in expression of β_1-adrenoceptors in the RV membrane

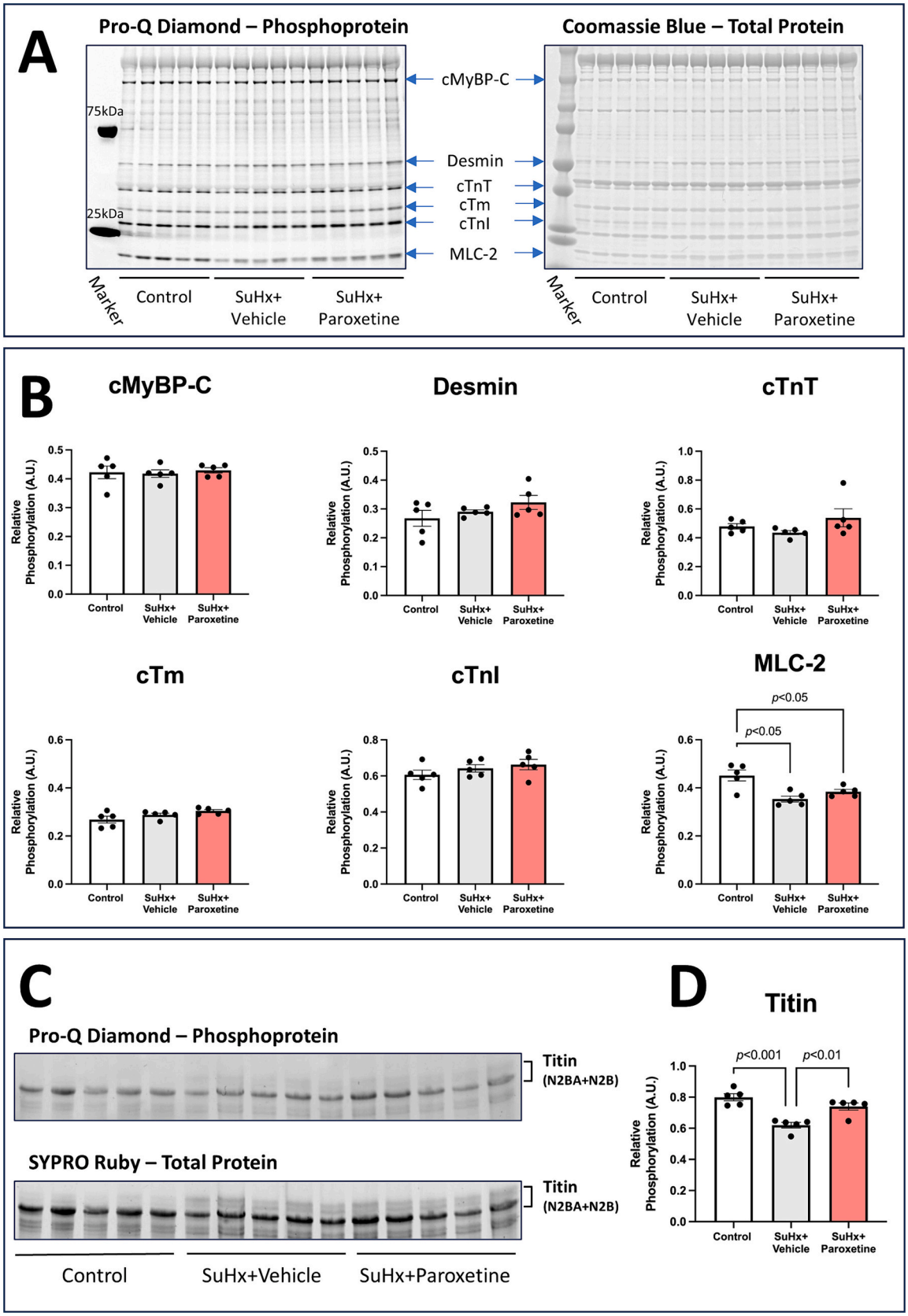

(caption on next page)

Fig. 4. Variable effects of chronic paroxetine treatment on the net phosphorylation status of myofilament proteins. **A:** Representative images of the same gradient (5–20 %) mini polyacrylamide gel stained with Pro-Q Diamond for phosphoprotein (left) and post-stained in Coomassie blue for total protein expression (right) for the determination of relative net phosphorylation of key myofilament proteins within the RV of Control ($n = 5$), SuHx+Vehicle (n = 5) and SuHx+Paroxetine (n = 5) rats. Blue arrows indicate the bands that were analyzed for the corresponding protein label. **B:** Quantification of the relative net phosphorylation status (phosphoprotein/total protein signal) of cMyBP-C, desmin, cTnT, cTm, cTnI and MLC-2. In general, the net phosphorylation of myofilament proteins was unchanged among the groups, apart from MLC-2, which was significantly reduced in both the vehicle- and paroxetine-treated (5 $mg{\cdot}kg^{-1}{\cdot}day^{-1}$) SuHx rats compared to Control rats. **C:** Representative images of the same 1 % agarose gel stained with Pro-Q Diamond for titin phosphoprotein (upper) and post-stained with SYPRO Ruby for titin total protein (lower) within the RV of Control ($n = 5$), SuHx+Vehicle (n = 5) and SuHx+Paroxetine (n = 5) rats. **D:** Quantification of the relative net phosphorylation status (phosphoprotein/total protein signal) of titin. PH in SuHx rats was associated with a significantly lower net titin phosphorylation compared to Control rats ($p < 0.001$). Chronic paroxetine treatment of SuHx rats resulted in significantly increased net titin phosphorylation relative to the vehicle-treated SuHx rats ($p < 0.01$). All samples were run simultaneously on one gel. Data are presented as mean ± SEM. A one-way ANOVA with a Bonferroni's post hoc test was used to assess differences between the groups. cMyBP-C: cardiac myosin binding protein-C, cTnT: cardiac troponin T, cTm: cardiac tropomyosin, cTnI: cardiac troponin I, MLC-2: myosin light chain-2. (For interpretation of the references to colour in this figure legend, the reader is referred to the web version of this article.)

fraction when compared to the control group (Fig. 6C), along with a significantly elevated RV tyrosine hydroxylase expression in both SuHx groups compared to controls (Fig. 6D). Furthermore, vehicle-treated SuHx rats exhibited significant depletion of the RV catecholamines, dopamine ($p < 0.01$ vs. Control, Fig. 6E) and norepinephrine ($p < 0.001$ vs. Control, Fig. 6F) when compared to control. Paroxetine treatment had no effect on the depletion of either dopamine ($p < 0.01$ vs. Control, Fig. 6E) or norepinephrine ($p < 0.001$ vs. Control, Fig. 6F) in the RV of SuHx rats. Interestingly, despite the levels of dopamine and norepinephrine in the RV of SuHx rats compared to control rats (Fig. 6E&F), no significant differences in RV epinephrine stores were found between the groups (Fig. 6G).

Overall, these data suggest that paroxetine exerts its beneficial effect upon RV systolic function and myofilament protein phosphorylation through a mechanism that is independent of GRK2 inhibition or modulation of the sympathetic nervous system.

4. Discussion

Here we report that chronic treatment of SuHx-induced PH in rats with the SSRI, paroxetine, significantly improves RV systolic myocardial function, reduces RV afterload and enhances RV-PA coupling, but with no effect on RV diastolic dysfunction. Greater net phosphorylation of titin and site-specific phosphorylation at MLC-$2v^{Ser15}$ was positively correlated with indices of RV systolic function (stroke volume, cardiac output and ejection fraction), suggesting that paroxetine induces its principal effect on the RV myocardium through changes in myofilament protein phosphorylation. We hypothesized that paroxetine would enhance RV myocardial function in the SuHx rats through suppression of GRK2 activation and subsequent restoration of physiological SNS and β-adrenergic signaling, ultimately driving the production of PKA within the cardiomyocytes. Despite the significant literature that supports this concept, we found the heightened GRK2 translocation from the cytosol to the membrane (used as an index of activity) in the RV of SuHx rats was not affected by chronic paroxetine treatment. Moreover, markedly elevated RV tyrosine hydroxylase levels and depletion of RV myocardial catecholamines (markers of SNS overactivation) were also unaffected by chronic paroxetine treatment of SuHx rats. In our study it appears that paroxetine exerted its beneficial effects upon the RV myocardium independent of GRK2 inhibition or attenuation of the SNS.

4.1. Improvements in RV systolic dysfunction without changes in RV hypertrophy or remodeling following chronic paroxetine treatment in PH rats

One of the key findings of our study is that chronic paroxetine treatment after the development of PH was able to significantly improve RV systolic function in the SuHx rats without affecting RV hypertrophy, myocardial remodeling (cardiomyocyte hypertrophy, myosin heavy chain/titin isoform switching), or the development of myocardial interstitial fibrosis that is consistently shown to be associated with chronic PH. Consistent with our study, others have reported that in both in a mouse myocardial infarction model [19] and a rat model of systemic hypertension [18] that chronic paroxetine treatment was able to prevent declines in LV systolic function. However, in contrast to our findings, both studies demonstrated that chronic paroxetine treatment also attenuated the development of cardiac hypertrophy and myocardial fibrosis [18,19]. Moreover, both studies showed that the beneficial effects of paroxetine in the LV myocardium is a result of direct GRK2 inhibition [18,19]. One of the main reasons as to why paroxetine had no effect on cardiac/cardiomyocyte hypertrophy despite improved RV systolic function is likely due to the differences in treatment strategy, as we opted for an intervention approach where paroxetine treatment began after PH was already established. Another important reason may be related to differences in the specific disease pathology. In the adaptive phase of RV remodeling in PH, it is thought that the expansion of the ECM and production/cross-linking of collagen serves to maintain the shape of the RV and prevent overstretch the cardiomyocytes and remodeling initially supports RV function against the greater afterload [33]. Given that in the present study, RV systolic pressures remained equally elevated in the vehicle-treated and paroxetine-treated SuHx rats indicates that the RV myocardial fibrosis and cardiomyocyte hypertrophy are most likely playing a supporting role in an attempt to preserve RV function. This indicates that paroxetine exerts its actions directly on the cardiomyocyte. Interestingly, a clinical study has also reported that in a cohort of cardiovascular disease-free subjects ($n = 4114$), that the use of SSRIs (including paroxetine) was associated with increased RV stroke volume and end diastolic volume along with a greater RV mass in male subjects, indicating that SSRIs may induce RV adaption and increase systolic performance specifically within the RV myocardium [34]. Taken together, it appears that paroxetine improves RV function and may further delay the progression of RV failure in the setting of PH via changes at the level of the myofilament.

4.2. Paroxetine preserved RV systolic function in PH rats potentially via enhanced myofilament phosphorylation

Accumulating evidence suggests that changes in post-translational modifications at the level of the myofilament and sarcomere contribute to the development of RV dysfunction and failure. In various models of PH and in RV tissue biopsies from PH patients, changes in phosphorylation of key myofilament proteins within the RV have been reported including titin, cMyBP-C, cTnT, cTnI and MLC-2v [10,35–37]. In the present study, we also found significant changes to the phosphorylation of key myofilament proteins, namely titin and MLC-2v in the RV myofilaments of SuHx rats compared to controls. Furthermore, we demonstrated that chronic paroxetine treatment increased relative phosphorylation of both titin and MLC-2v. Most importantly however, is that relative phosphorylation state of both titin and MLC-2v correlated with RV systolic indices such as stroke volume, cardiac output and ejection fraction, suggesting that the elevated phosphorylation status of both of these proteins likely contributes to the improvements in RV systolic function associated with chronic paroxetine treatment.

MLC-2v resides within the myosin neck region and plays a critical

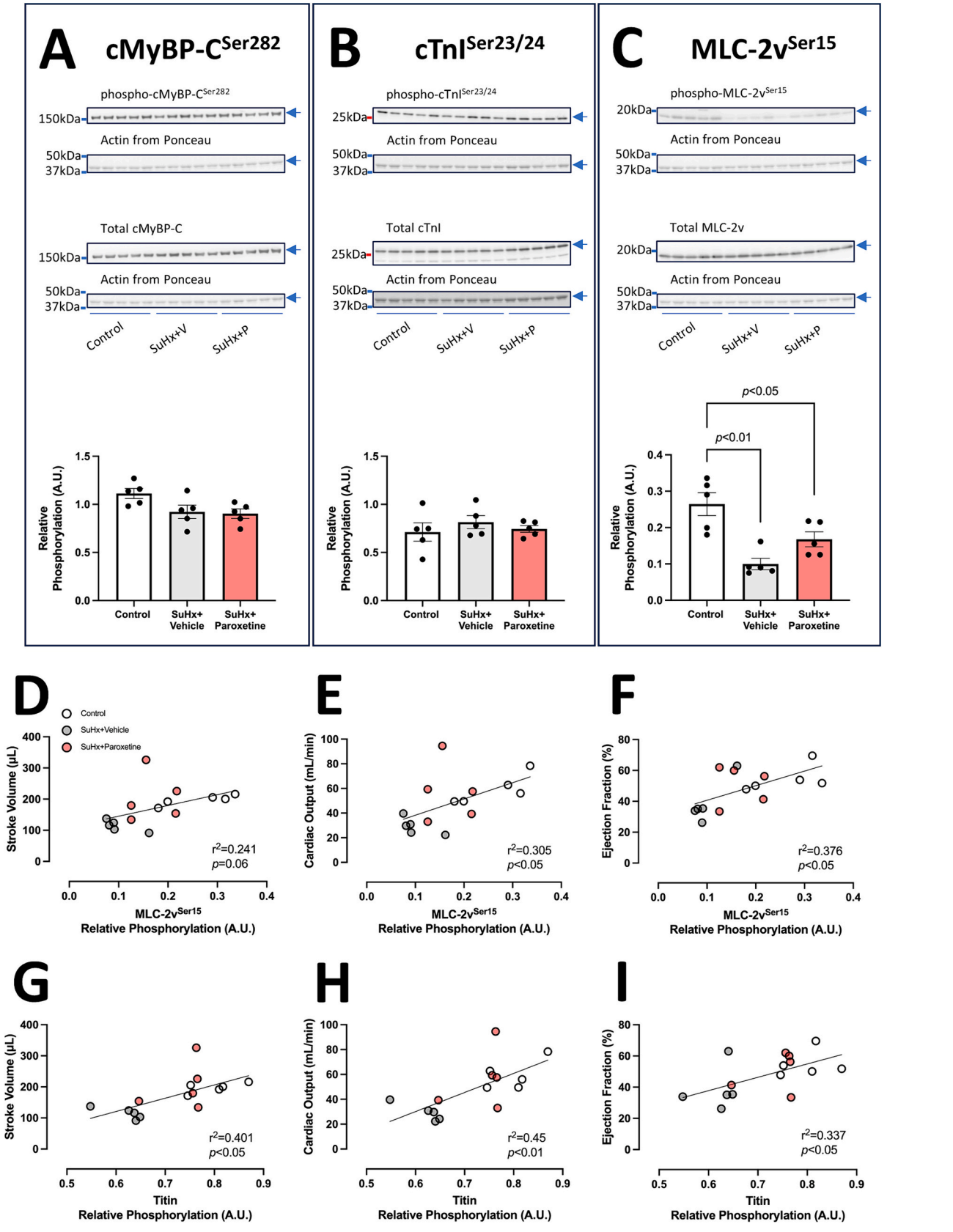

(caption on next page)

Fig. 5. Chronic paroxetine treatment was associated with greater MLC-2v phosphorylation in RV of SuHx rats that correlated with improved RV systolic function. **A:** Representative images of Western blot membranes for phospho-cMyBP-C^{Ser282} and total cMyBP-C along with the respective actin bands from Ponceau-S staining that served as the loading control for RV myofilament samples from Control ($n = 5$), SuHx+Vehicle (n = 5) and SuHx+Paroxetine (n = 5) rats. **B:** Representative images of Western blot membranes for phospho-cTnI$^{Ser23/24}$ and total cTnI along with the respective actin bands from Ponceau-S staining for RV myofilament samples from Control (n = 5), SuHx+Vehicle (n = 5) and SuHx+Paroxetine (n = 5) rats. No significant differences in either relative cMyBP-C^{Ser282} phosphorylation or relative cTnI$^{Ser23/24}$ phosphorylation was observed between the groups. **C:** Representative images of Western blot membranes for phospho-MLC-2v^{Ser15} and total MLC-2v along with the respective actin bands from Ponceau-S staining for RV myofilament samples from Control ($n = 5$), SuHx+Vehicle (n = 5) and SuHx+Paroxetine (n = 5) rats. PH in the SuHx rats resulted in a significantly lower MLC-2v^{Ser15} phosphorylation compared to Control rats, whereas paroxetine treatment of SuHx rats (5 mg·kg^{-1}·day^{-1}) resulted in an ~70 % greater MLC-2v^{Ser15} phosphorylation compared to vehicle-treated SuHx rats. All samples were run on one gel, and for relative phosphorylation experiments gels and membranes for phospho- and total protein were run in parallel and processed under the same conditions. **A** and **C** share the same loading control as they were blotted from separate parts of the same original membrane. Numbers along the left border of the Western blot images in **A**, **B** and **C** represent the position of the molecular weight marker on the membrane. Blue arrows in the Western blot images in **A**, **B** and **C** indicate the bands that were analyzed. Data are presented as mean ± SEM. A one-way ANOVA with a Bonferroni's post hoc test was used to assess differences between the groups. **D, E & F:** Scatter plots representing the relationship between RV myofilament MLC-2v^{Ser15} relative phosphorylation and RV stroke volume (**D**), cardiac output (**E**) and ejection fraction (**F**) in Control ($n = 5$), SuHx+Vehicle (n = 5) and SuHx+Paroxetine (n = 5) rats. **G, H & I:** Scatter plots representing the relationship between RV myofilament net titin phosphorylation and RV stroke volume (**G**), cardiac output (**H**) and ejection fraction (**I**) in the same rats as D & F. In general, there was a positive and significant correlation between RV MLC-2v^{Ser15} and net titin phosphorylation with the indices of RV systolic function. For **D**—**I**, pooled linear regression analysis was used to establish correlations between the independent and dependent variables. cMyBP-C: cardiac myosin binding protein-C, cTnI: cardiac troponin I, MLC-2v: myosin light chain-2 ventricular isoform, SuHx+V: SuHx+Vehicle, SuHx+P: SuHx+Paroxetine. (For interpretation of the references to colour in this figure legend, the reader is referred to the web version of this article.)

role in regulating the conformation and binding of myosin heads to actin and therefore, cardiac contraction and relaxation [38,39]. When phosphorylated by MLC kinase at serine 15, myosin heads shift from the region of the myosin backbone (i.e. the super-relaxed (SRX) state) towards the actin thin-filament binding sites (i.e. the disordered-relaxed (DRX) state) and thereby increase the rate of force development and accelerate cross-bridge recruitment [40]. At the whole heart level, this translates into enhanced ventricular systolic function. Recently, it has been demonstrated that increasing MLC-2v phosphorylation through activation of MLC kinase promotes the transition of myosin heads from the SRX state to the contraction-ready DRX state, resulting in improved systolic function in mice [41]. Our group has also recently found that in the RV of rats with SuHx-induced PH, albeit at an earlier timepoint, that a greater number of myosin heads are in the SRX state at end diastole [20], making them unavailable for actin-myosin cross-bridge binding in the subsequent contraction. While not tested in this study, it is therefore conceivable that the greater relative MLC-2v phosphorylation associated with chronic paroxetine treatment in the SuHx rats in our study promotes the transition of myosin from the SRX to DRX state during the diastolic phase, increasing the number of strong cross-bridges formed during the systolic contraction and thereby improving global RV systolic function.

Titin is a 4MDa giant protein that spans half the sarcomere from the *Z*-disc to M-line. Titin acts like a spring within the sarcomere and primarily functions to modulate cardiomyocyte compliance during ventricular filling [42], although it also interacts with the myosin thick-filament to regulate myosin head flexibility and extension [43]. The phosphorylation sites within the titin protein are numerous, and specific sites affect titin's function based on location and the phosphorylating kinase [44]. In the present study, we showed that the net phosphorylation of titin was reduced in the RV of PH rats, consistent with previous studies [10,45], and paroxetine treatment resulted in greater titin phosphorylation. As we did not measure site-specific phosphorylation of titin (requiring custom antibodies), we can only speculate as to how greater titin phosphorylation would improve RV systolic function. One possibility is that increased titin compliance as a result of greater net phosphorylation could allow for greater recruitment of the Frank-Starling reserve that subsequently facilitates improvements in RV systolic function. In this study however, we observed only modest shifts in RV end diastolic volume. Future studies that induce the myocardial stretch response are required to further elucidate this mechanism.

The regulation of myofilament protein phosphorylation is indeed complex and the interplay between the thick- and thin-filament associated proteins and titin is tightly regulated to maintain cardiac contraction and relaxation. How paroxetine affects these specific proteins to influence RV cardiomyocyte contractility and relaxation certainly warrants further investigation.

4.3. The beneficial effects of paroxetine upon the RV myocardium in PH rats independent of the sympathetic nervous system

We had initially hypothesized that chronic paroxetine treatment of SuHx rats would exert its beneficial effects upon the RV through inhibition of GRK2 and subsequent attenuation of SNS overactivation. Much to our surprise, paroxetine did not prevent GRK2 membrane translocation, changes in tyrosine hydroxylase expression or RV myocardial catecholamine depletion. Therefore, based on our hypothesis and the data obtained in this study, we cannot identify the specific molecular mechanism by which paroxetine improved myofilament protein phosphorylation and global RV systolic function, which is a limitation of this study. Nevertheless, paroxetine has been reported to have pleiotropic effects beyond the inhibition of serotonin reuptake and GRK2, which may provide insights to a potential mechanism, in particular relating to oxidative stress. In the brain of rats, paroxetine has been reported to interact directly with mitochondrial proteins to prevent the development of mitochondrial-derived oxidative stress and inducible nitric oxide synthase (iNOS)-derived inflammation, independent of its actions on the serotonin transporter [46]. Another study has also reported paroxetine acts as a mitochondrial superoxide scavenger in cultured vascular endothelial cells, with this mechanism preventing the development of endothelial dysfunction in a rat model of diabetes mellitus [47]. Moreover, chronic paroxetine treatment of rats post-myocardial infarction significantly reduced myocardial reactive oxygen species (ROS) that was associated with improved LV systolic function [48]. The fact that paroxetine can directly inhibit ROS/iNOS to reduced oxidative/nitrosative stress is very important, given that oxidative/nitrosative stress plays a central role in the evolution of heart failure in general [49,50], but also RV dysfunction and failure in the setting of PH [51]. At the level of the sarcomere, ROS can induce numerous post-translational modifications upon all of the major myofilament proteins that not only results in impaired myofilament function [50], but also contributes to global myocardial dysfunction and failure [52]. Indeed, in a mouse model of RV failure, elevated ROS-induced oxidation of RV myofilament proteins was associated with reduced ex-vivo force development of RV trabeculae that correlated with reduced RV systolic function [53]. We did not evaluate RV oxidative stress/antioxidant capacity status or myofilament post-translational modifications related to ROS/reactive nitrogen species in our study, which is another limitation. However, it is plausible that paroxetine through its ability to inhibit mitochondrial sources of ROS and inflammation, may also improve RV systolic function by preventing the oxidation of myofilament proteins as well as bolstering the activity of kinases that phosphorylate these myofilament

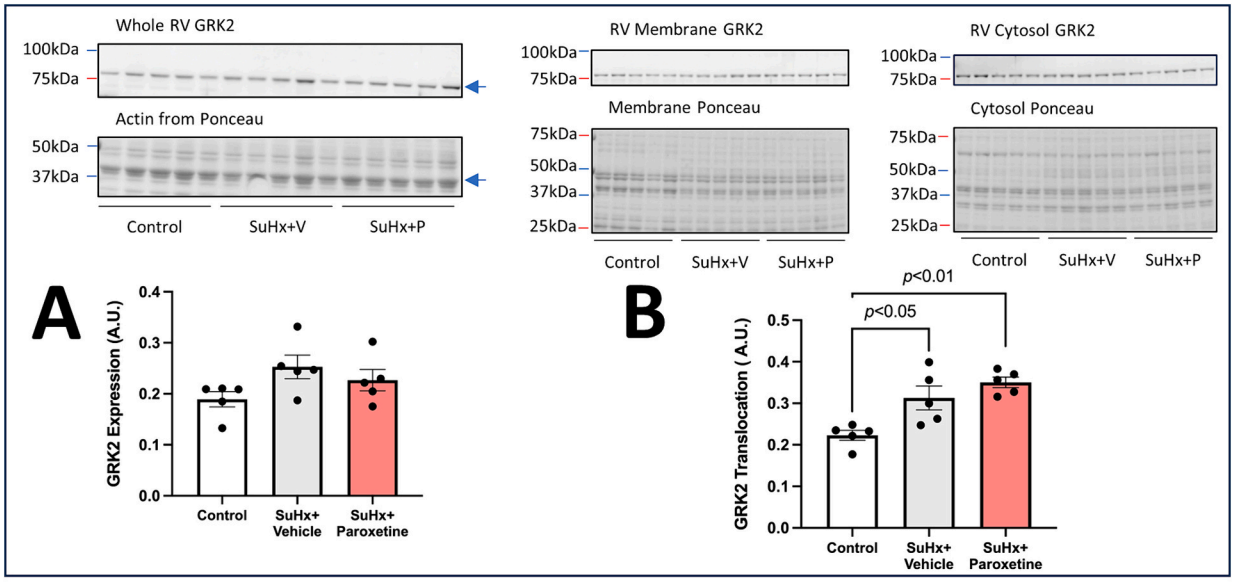

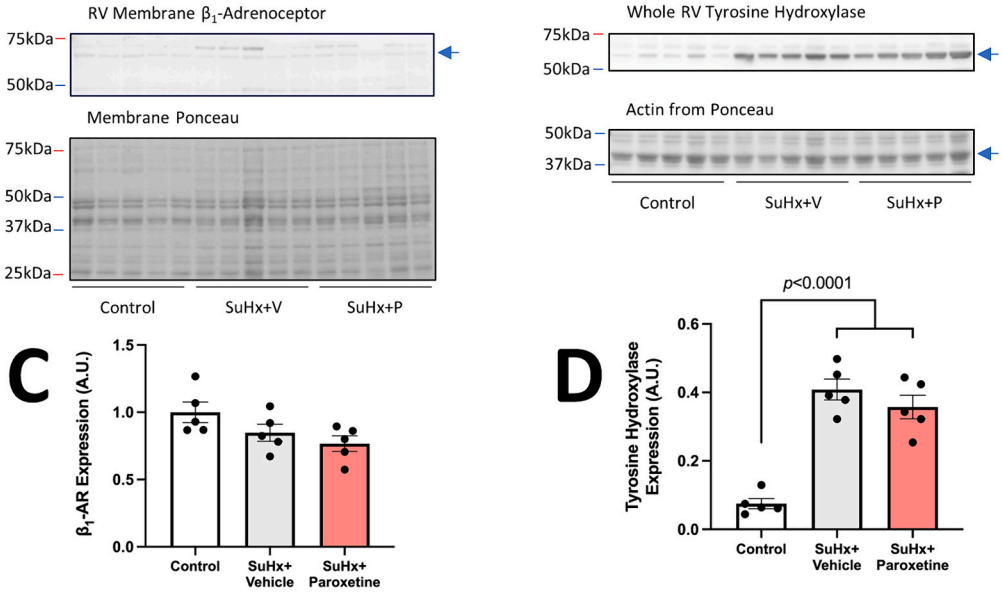

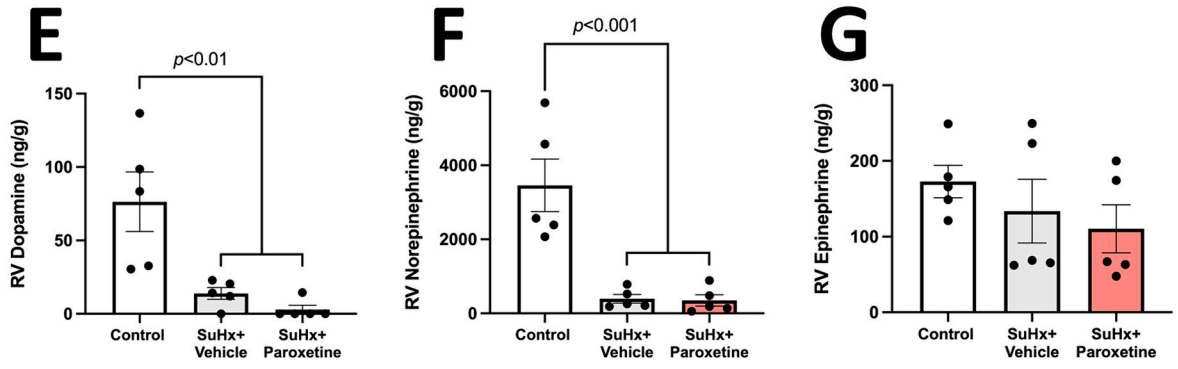

(caption on next page)

Fig. 6. The beneficial effects of chronic paroxetine treatment upon RV myofilament protein phosphorylation and RV systolic function appeared to be independent of GRK2 inhibition and attenuation of sympathetic nervous system (SNS) activation. **A:** Representative images of Western blot membranes for GRK2 and the corresponding actin bands from the Ponceau-S staining that served as the loading control for whole RV samples from Control ($n = 5$), SuHx+Vehicle (n = 5) and SuHx+Paroxetine (n = 5) rats. GRK2 expression was ~20–30 % higher in both SuHx groups compared to Control (NS). **B:** Representative images of Western blot membranes for GRK2 from the membrane and cytosolic fractions and the respective Ponceau-S staining for each fraction in the same rats as A. PH in SuHx rats was associated with a significant increase in GRK2 translocation ($p < 0.05$ vs. Control) that was unaffected by chronic paroxetine treatment (5 $mg{\cdot}kg^{-1}{\cdot}day^{-1}$, $p < 0.01$ vs. Control). Translocation was calculated as the ratio of membrane to cytosolic expression of GRK2. **C:** Representative images of Western membranes for β_1-adrenoceptors and the respective Ponceau-S staining for the RV membrane fractions from the same rats as A. There were no appreciable differences in β_1-adrenoceptor expression in the RV membrane fraction between the groups. **D:** Representative images of Western blot membranes for tyrosine hydroxylase and the corresponding actin bands from the Ponceau-S staining for whole RV samples from Control (n = 5), SuHx+Vehicle (n = 5) and SuHx+Paroxetine (n = 5) rats. RV tyrosine hydroxylase expression was significantly increased in both groups of SuHx rats compared to the control group (both $p < 0.0001$). Numbers along the left border of the Western blot images in **A**, **B**, **C & D** represent the position of the molecular weight marker on the membrane. Blue arrows in the Western blot images in **A**, **B**, **C & D** indicate the bands that were analyzed. All samples were run on one gel and for the translocation experiments, gels and membranes were run in parallel and processed under the same conditions. **E, F & G:** RV catecholamine levels as measured by HPLC in Control (n = 5), SuHx+Vehicle (n = 5) and SuHx+Paroxetine (n = 5) rats. Compared to Control, both groups of SuHx rats exhibited significantly lower levels of dopamine (**E**, both $p < 0.01$) and norepinephrine (**F**, both $p < 0.001$), whereas there were no differences among the groups for RV epinephrine levels (**G**). Data are presented as mean ± SEM. A one-way ANOVA with a Bonferroni's post hoc test was used to assess differences between the groups. SuHx+V: SuHx+Vehicle, SuHx+P: SuHx+Paroxetine. (For interpretation of the references to colour in this figure legend, the reader is referred to the web version of this article.)

proteins and as such, this will be the focus of our future studies.

4.4. Other study limitations

Other than those mentioned above, our study has some further limitations that also need to be addressed. First, paroxetine did not attenuate the RV diastolic dysfunction associated with PH in our study. Diastolic dysfunction is a major contributor to the development of RV failure in PH patients, with clinical evidence suggesting that RV diastolic dysfunction is a sensitive marker of PH progression and patient survival [36,54]. Paroxetine, through a GRK2-dependent mechanism, was able to prevent the significant elevation of LV end diastolic pressure and enhance LV diastolic functional reserve in a mouse model of myocardial infarction [19]. In our study we only observed an improvement of RV systolic function that appeared to occur independently of a GRK2 inhibitory mechanism. Taken with the previous study [19], this suggests that the inhibition of GRK2 may be required for paroxetine to improve diastolic function. On the other hand, it has been suggested that enhancing ventricular-arterial coupling and reducing ventricular afterload, interventions that improve systolic function (e.g. paroxetine) could indirectly mitigate the progression of diastolic dysfunction by reducing the burden upon the RV [55]. Therefore, a future study that adopts a longer-term paroxetine treatment protocol or a prevention study design is certainly warranted (see below). Moreover, during the hemodynamic analysis, rats were not subjected to any form of cardiac challenge such as volume loading or a dobutamine stress test. We refrained from such an approach to avoid confounding analyses relating to the phosphorylation of RV myofilament proteins namely, cMyBP-C, cTnI and titin that are key targets for PKA stimulation. However, by performing such tests we could have gained more insight into the systolic and diastolic functional reserves of the RV in addition to the β-adrenergic sensitivity of the myocardium. Second, given the SuHx model of PH is not purely a model of RV dysfunction, but rather RV dysfunction and eventual failure secondary to lung vascular remodeling [56], another limitation is that we did not evaluate pulmonary vascular remodeling. Nevertheless, as there were no differences between the vehicle- and paroxetine-treated SuHx rats in terms of the RV systolic pressure, reflecting pulmonary artery pressure, we believe it unlikely that chronic paroxetine treatment had an appreciable effect upon the pulmonary vascular remodeling associated with PH in this model.

Additionally, and as mentioned above, we opted only for an interventional study design whereby paroxetine was administered once PH was fully established, which is another limitation of our study. A prevention study design (i.e. paroxetine administration from the beginning of the hypoxic period) will also be required in a future study to properly ascertain the potential benefits of paroxetine to improve both RV systolic and diastolic function in the setting of PH and gain more insight to the clinical translatability of paroxetine. Moreover, we did not include a paroxetine-treated control group in our proof-of-concept study and this is also another limitation of this study. Given that it has been reported that SSRIs (including paroxetine) may directly enhance RV systolic myocardial function in cardiovascular disease-free subjects [34], it is important in our future studies to include a paroxetine-treated control group to obtain further mechanistic insights as to how paroxetine may improve myocardial function.

5. Conclusions

Our study aimed to investigate if chronic paroxetine treatment would improve RV myocardial function via the inhibition of GRK2 and subsequently prevent changes in the phosphorylation status of key myofilament proteins in a rat model of PH. Surprisingly and contrary to our initial hypothesis, paroxetine improved RV systolic function, RV-PA coupling and myofilament protein phosphorylation in the SuHx-induced rat model of PH but seemingly through a GRK2-independent mechanism. Although we can only speculate at this stage, it seems likely that the reported antioxidant mechanisms of paroxetine may drive improvements at the level of the myofilament and global RV function. Although this study provides important preliminary information regarding the actions of paroxetine upon the RV in the setting of PH, detailed mechanistic investigations are required.

Funding information

This study was supported by Investigator Initiated Study grants from Janssen Pharmaceuticals (M.T.W., T.O.) and Nippon Shinyaku Co. (T.O.) and a Grant-in-Aid for Scientific Research from the Japan Society for the Promotion of Science (19K16498 and 22K15368; M.T.W.). V.S. was supported by an Invitational Fellowship from the Japan Society for the Promotion of Science (S23089).

Ethics statement

Experiments involving animals were conducted in accordance with the guidelines set by the Physiological Society of Japan and the National Research Council's Guide for the Care and Use of Laboratory Animals. Experiments were approved by the local animal experimentation committee at the National Cerebral and Cardiovascular Center (Proposal No. 19053, 20010, 21048, 22080 and 23083). Reporting of animal studies in this article is in accordance with the ARRIVE guidelines for animal research.

CRediT authorship contribution statement

Mark T. Waddingham: Writing – review & editing, Writing – original draft, Visualization, Validation, Project administration, Methodology, Investigation, Funding acquisition, Formal analysis, Data curation, Conceptualization. **Hirotsugu Tsuchimochi:** Writing – review & editing, Validation, Methodology, Investigation. **Takashi Sonobe:** Validation, Methodology, Investigation, Formal analysis. **Vasco Sequeira:** Writing – review & editing, Methodology. **Md Junayed Nayeem:** Visualization, Investigation. **Mikiyasu Shirai:** Supervision, Methodology, Conceptualization. **James T. Pearson:** Writing – review & editing, Validation, Supervision, Resources, Methodology, Conceptualization. **Takeshi Ogo:** Writing – review & editing, Validation, Supervision, Resources, Methodology, Funding acquisition, Conceptualization.

Declaration of competing interest

Takeshi Ogo reports financial support was provided by Janssen Pharmaceutical KK. Takeshi Ogo reports financial support was provided by Nippon Shinyaku Co Ltd. Mark T. Waddingham reports financial support was provided by Japan Society for the Promotion of Science. Takeshi Ogo reports a relationship with Janssen Pharmaceutical KK that includes: speaking and lecture fees. Takeshi Ogo reports a relationship with Nippon Shinyaku Co Ltd. that includes: speaking and lecture fees. Takeshi Ogo reports a relationship with Bayer Yakuhin Kabushiki Kaisha that includes: speaking and lecture fees. If there are other authors, they declare that they have no known competing financial interests or personal relationships that could have appeared to influence the work reported in this paper.

Acknowledgements

We thank Nozomi Tokuhara for support with the animal experiments.

Appendix A. Supplementary data

Supplementary data to this article can be found online at https://doi.org/10.1016/j.jmccpl.2024.100072.

References

[1] Thenappan T, Ormiston ML, Ryan JJ, Archer SL. Pulmonary arterial hypertension: pathogenesis and clinical management. BMJ 2018:360.
[2] Vonk-Noordegraaf A, Haddad F, Chin KM, Forfia PR, Kawut SM, Lumens J, et al. Right heart adaptation to pulmonary arterial hypertension: physiology and pathobiology. J. Am. Coll. Cardiol. 2013;62(25, Supplement):D22–33.
[3] Badagliacca R, Mercurio V, Romeo E, Correale M, Masarone D, Papa S, et al. Beta-blockers in pulmonary arterial hypertension: time for a second thought? Vasc. Pharmacol. 2022;144:106974.
[4] Grinnan D, Bogaard H-J, Grizzard J, Tassell BV, Abbate A, DeWilde C, et al. Treatment of group i pulmonary arterial hypertension with carvedilol is safe. Am. J. Respir. Crit. Care Med. 2014;189(12):1562–4.
[5] de Man FS, Handoko ML, van Ballegoij JJM, Schalij I, Bogaards SJP, Postmus PE, et al. Bisoprolol delays progression towards right heart failure in experimental pulmonary hypertension. Circulation. Heart Failure 2012;5(1):97–105.
[6] Lima-Seolin Bgd, Colombo R, Bonetto JHP, Teixeira RB, Donatti LM, Casali KR, et al. Bucindolol improves right ventricle function in rats with pulmonary arterial hypertension through the reversal of autonomic imbalance. Eur. J. Pharmacol. 2017;798:57–65.
[7] Perros F, Ranchoux B, Izikki M, Bentebbal S, Happé C, Antigny F, et al. Nebivolol for improving endothelial dysfunction, pulmonary vascular remodeling, and right heart function in pulmonary hypertension. J. Am. Coll. Cardiol. 2015;65(7):668–80.
[8] Bogaard HJ, Natarajan R, Mizuno S, Abbate A, Chang PJ, Chau VQ, et al. Adrenergic receptor blockade reverses right heart remodeling and dysfunction in pulmonary hypertensive rats. Am. J. Respir. Crit. Care Med. 2010;182(5):652–60.
[9] Rain S, Handoko ML, Vonk Noordegraaf A, Bogaard HJ, van der Velden J, de Man FS. Pressure-overload-induced right heart failure. Pflugers Arch. - Eur. J. Physiol. 2014;466(6):1055–63.
[10] Rain S, Bos DdSG, Handoko ML, Westerhof N, Stienen G, Ottenheijm C, et al. Protein changes contributing to right ventricular cardiomyocyte diastolic dysfunction in pulmonary arterial hypertension. J. Am. Heart Assoc. 2014;3(3).
[11] Ferrero KM, Koch WJ. Grk2 in cardiovascular disease and its potential as a therapeutic target. J. Mol. Cell. Cardiol. 2022;172:14–23.
[12] Murga C, Arcones AC, Cruces-Sande M, Briones AM, Salaices M, Mayor Jr F. G protein-coupled receptor kinase 2 (grk2) as a potential therapeutic target in cardiovascular and metabolic diseases. Front. Pharmacol. 2019;10(112).
[13] Pfleger J, Gross P, Johnson J, Carter RL, Gao E, Tilley DG, et al. G protein-coupled receptor kinase 2 contributes to impaired fatty acid metabolism in the failing heart. J. Mol. Cell. Cardiol. 2018;123:108–17.
[14] Sato PY, Chuprun JK, Ibetti J, Cannavo A, Drosatos K, Elrod JW, et al. Grk2 compromises cardiomyocyte mitochondrial function by diminishing fatty acid-mediated oxygen consumption and increasing superoxide levels. J. Mol. Cell. Cardiol. 2015;89:360–4.
[15] Cannavo A, Koch WJ. Grk2 as negative modulator of no bioavailability: implications for cardiovascular disease. Cell. Signal. 2018;41:33–40.
[16] Piao L, Fang YH, Parikh KS, Ryan JJ, D'Souza KM, Theccanat T, et al. Grk2-mediated inhibition of adrenergic and dopaminergic signaling in right ventricular hypertrophy: therapeutic implications in pulmonary hypertension. Circulation 2012;126(24):2859–69.
[17] Thal DM, Homan KT, Chen J, Wu EK, Hinkle PM, Huang ZM, et al. Paroxetine is a direct inhibitor of g protein-coupled receptor kinase 2 and increases myocardial contractility. ACS Chem. Biol. 2012;7(11):1830–9.
[18] Sun X, Zhou M, Wen G, Huang Y, Wu J, Peng L, et al. Paroxetine attenuates cardiac hypertrophy via blocking grk2 and adrb1 interaction in hypertension. J. Am. Heart Assoc. 2021;10(1):e016364.
[19] Schumacher SM, Gao E, Zhu W, Chen X, Chuprun JK, Feldman AM, et al. Paroxetine-mediated grk2 inhibition reverses cardiac dysfunction and remodeling after myocardial infarction. Sci. Transl. Med. 2015;7(277):277ra31-ra31.
[20] Waddingham MT, Tsuchimochi H, Sonobe T, Asano R, Jin H, Ow CPC, et al. Using synchrotron radiation imaging techniques to elucidate the actions of hexarelin in the heart of small animal models. Front. Physiol. 2022;12.
[21] Miranda-Silva D, Sequeira V, Lourenço AP, Falcão-Pires I. Assessing rodent cardiac function in vivo using hemodynamic pressure-volume loops. Front. Physiol. 2022;12.
[22] Potus F, Hindmarch CCT, Dunham-Snary KJ, Stafford J, Archer SL. Transcriptomic signature of right ventricular failure in experimental pulmonary arterial hypertension: deep sequencing demonstrates mitochondrial, fibrotic, inflammatory and angiogenic abnormalities. Int. J. Mol. Sci. 2018;19(9):2730.
[23] Ogilvie LM, Edgett BA, Huber JS, Platt MJ, Eberl HJ, Lutchmedial S, et al. Hemodynamic assessment of diastolic function for experimental models. Am. J. Phys. Heart Circ. Phys. 2020;318(5). H1139-H58.
[24] Waddingham MT, Sonobe T, Tsuchimochi H, Edgley AJ, Sukumaran V, Chen YC, et al. Diastolic dysfunction is initiated by cardiomyocyte impairment ahead of endothelial dysfunction due to increased oxidative stress and inflammation in an experimental prediabetes model. J. Mol. Cell. Cardiol. 2019;137:119–31.
[25] Capote AE, Batra A, Warren CM, Chowdhury SAK, Wolska BM, Solaro RJ, et al. B-arrestin-2 signaling is important to preserve cardiac function during aging. Front. Physiol. 2021;12.
[26] Warren CM, Krzesinski PR, Greaser ML. Vertical agarose gel electrophoresis and electroblotting of high-molecular-weight proteins. Electrophoresis 2003;24(11):1695–702.
[27] Warren CM, Greaser ML. Method for cardiac myosin heavy chain separation by sodium dodecyl sulfate gel electrophoresis. Anal. Biochem. 2003;320(1):149–51.
[28] Pearson James T, Thambyah Hamish P, Waddingham Mark T, Inagaki T, Sukumaran V, Ngo Jennifer P, et al. B-blockade prevents coronary macro- and microvascular dysfunction induced by a high salt diet and insulin resistance in the goto–kakizaki rat. Clin. Sci. 2021;135(2):327–46.
[29] Cingolani OH, Kass DA. Pressure-volume relation analysis of mouse ventricular function. Am. J. Phys. Heart Circ. Phys. 2011;301(6). H2198-H206.
[30] Trip P, Rain S, Handoko ML, van der Bruggen C, Bogaard HJ, Marcus JT, et al. Clinical relevance of right ventricular diastolic stiffness in pulmonary hypertension. Eur. Respir. J. 2015;45(6):1603–12.
[31] Burkhoff D, Mirsky I, Suga H. Assessment of systolic and diastolic ventricular properties via pressure-volume analysis: a guide for clinical, translational, and basic researchers. Am. J. Physiol. Heart Circ. Physiol. 2005;289(2):H501–12.
[32] Vanderpool RR, Puri R, Osorio A, Wickstrom K, Desai AA, Black SM, et al. Surfing the right ventricular pressure waveform: methods to assess global, systolic and diastolic rv function from a clinical right heart catheterization. Pulmon. Circ. 2020;10(1):2045894019850993.
[33] Andersen S, Nielsen-Kudsk JE, Noordegraaf AV, Man Fsd. Right ventricular fibrosis. Circulation 2019;139(2):269–85.
[34] Ventetuolo CE, Barr RG, Bluemke DA, Jain A, Delaney JAC, Hundley WG, et al. Selective serotonin reuptake inhibitor use is associated with right ventricular structure and function: the mesa-right ventricle study. PLoS One 2012;7(2):e30480.
[35] Cowley PM, Wang G, Chang AN, Makwana O, Swigart PM, Lovett DH, et al. The α1a-adrenergic receptor subtype mediates increased contraction of failing right ventricular myocardium. Am. J. Phys. Heart Circ. Phys. 2015;309(5). H888-H96.
[36] Rain S, Handoko ML, Trip P, Gan CT-J, Westerhof N, Stienen GJ, et al. Right ventricular diastolic impairment in patients with pulmonary arterial hypertension. Circulation 2013;128(18):2016–25.
[37] Walker LA, Walker JS, Glazier A, Brown DR, Stenmark KR, Buttrick PM. Biochemical and myofilament responses of the right ventricle to severe pulmonary hypertension. Am. J. Physiol. Heart Circ. Physiol. 2011;301(3). H832-H40.

[38] Moss RL, Fitzsimons DP. Myosin light chain 2 into the mainstream of cardiac development and contractility. Circ. Res. 2006;99(3):225–7.
[39] Kampourakis T, Sun Y-B, Irving M. Myosin light chain phosphorylation enhances contraction of heart muscle via structural changes in both thick and thin filaments. Proc. Natl. Acad. Sci. 2016;113(21). E3039-E47.
[40] Colson BA, Locher MR, Bekyarova T, Patel JR, Fitzsimons DP, Irving TC, et al. Differential roles of regulatory light chain and myosin binding protein-c phosphorylations in the modulation of cardiac force development. J. Physiol. 2010; 588(Pt 6):981–93.
[41] Hitsumoto T, Tsukamoto O, Matsuoka K, Li J, Liu L, Kuramoto Y, et al. Restoration of cardiac myosin light chain kinase ameliorates systolic dysfunction by reducing superrelaxed myosin. Circulation 2023;147(25):1902–18.
[42] Linke WA, Hamdani N. Gigantic business: titin properties and function through thick and thin. Circ. Res. 2014;114(6):1052–68.
[43] Hanft LM, Greaser ML, McDonald KS. Titin-mediated control of cardiac myofibrillar function. Arch. Biochem. Biophys. 2014;552–553:83–91.
[44] Hamdani N, Herwig M, Linke WA. Tampering with springs: phosphorylation of titin affecting the mechanical function of cardiomyocytes. Biophys. Rev. 2017;9(3): 225–37.
[45] Rain S, Andersen S, Najafi A, Gammelgaard Schultz J, da Silva Gonçalves Bós D, Handoko ML, et al. Right ventricular myocardial stiffness in experimental pulmonary arterial hypertension. Relative Contribution of Fibrosis and Myofibril Stiffness 2016;9(7).
[46] Steiner JP, Bachani M, Wolfson-Stofko B, Lee M-H, Wang T, Li G, et al. Interaction of paroxetine with mitochondrial proteins mediates neuroprotection. Neurotherapeutics 2015;12(1):200–16.
[47] Gerö D, Szoleczky P, Suzuki K, Módis K, Oláh G, Coletta C, et al. Cell-based screening identifies paroxetine as an inhibitor of diabetic endothelial dysfunction. Diabetes 2013;62(3):953–64.
[48] Lassen TR, Nielsen JM, Johnsen J, Ringgaard S, Botker HE, Kristiansen SB. Effect of paroxetine on left ventricular remodeling in an in vivo rat model of myocardial infarction. Basic Res. Cardiol. 2017;112(3):26.
[49] Sumandea MP, Steinberg SF. Redox signaling and cardiac sarcomeres. J. Biol. Chem. 2011;286(12):9921–7.
[50] Steinberg SF. Oxidative stress and sarcomeric proteins. Circ. Res. 2013;112(2): 393–405.
[51] Mikhael M, Makar C, Wissa A, Le T, Eghbali M, Umar S. Oxidative stress and its implications in the right ventricular remodeling secondary to pulmonary hypertension. Front. Physiol. 2019;10.
[52] Canton M, Menazza S, Sheeran FL, Polverino de Laureto P, Di Lisa F, Pepe S. Oxidation of myofibrillar proteins in human heart failure. J. Am. Coll. Cardiol. 2011;57(3):300–9.
[53] Cowley PM, Wang G, Swigart PM, Raghunathan A, Reddy N, Dulam P, et al. Reversal of right ventricular failure by chronic α1a-subtype adrenergic agonist therapy. Am. J. Phys. Heart Circ. Phys. 2019;316(1). H224-H32.
[54] Swift AJ, Capener D, Johns C, Hamilton N, Rothman A, Elliot C, et al. Magnetic resonance imaging in the prognostic evaluation of patients with pulmonary arterial hypertension. Am. J. Respir. Crit. Care Med. 2017;196(2):228–39.
[55] Borlaug BA, Kass DA. Invasive hemodynamic assessment in heart failure. Heart Fail. Clin. 2009;5(2):217–28.
[56] Abe K, Toba M, Alzoubi A, Ito M, Fagan KA, Cool CD, et al. Formation of plexiform lesions in experimental severe pulmonary arterial hypertension. Circulation 2010; 121(25):2747–54.